Summer 2023

Dynamics and Timescales of Magmatic Processes at Cerro Uturuncu, Bolivia

Sarah Jane Rasor
Missouri State University, sr87s@MissouriState.edu

Recommended Citation

DYNAMICS AND TIMESCALES OF MAGMATIC PROCESSES AT CERRO

UTURUNCU, BOLIVIA

A Master's Thesis

Presented to

The Graduate College of

Missouri State University

In Partial Fulfillment

Of the Requirements for the Degree

Master of Science, Geography and Geology

By

Sarah Jane Rasor

August 2023

DYNAMICS AND TIMESCALES OF MAGMATIC PROCESSES AT CERRO UTURUNCU, BOLIVIA

Geography, Geology, and Planning

Missouri State University, August 2023

Master of Science

Sarah Jane Rasor

ABSTRACT

Between 12-25°S latitude there is prolific volcanism fueled by the Altiplano-Puna Magmatic Body (APMB), a mid-crustal magma body above the 30° angle subduction of the Nazca plate and within 60-70 km thick South American crust. Cerro Uturuncu, a stratovolcano constructed above the center of the APMB, can provide insight to the evolution of the APMB over time. Previous research suggests that the APMB is more homogenous near its center as opposed to its edges. However, the processes that led to greater homogenization as well as the structure of the magma body below Cerro Uturuncu remain unknown. This research contributes greater understanding to the homogenization of and mixing within the APMB and comments on how this relates to magma architecture and residence times. While previous research on Cerro Uturuncu has focused on whole- rock geochemistry, this research evaluates sub-crystal plagioclase geochemistry and geochronometry. Textural classification, major and trace element analysis, and Sr diffusion modeling were performed on eight Cerro Uturuncu samples representing the four largest lava stages in recent Cerro Uturuncu history (1 Ma) using optical microscopy, LA-ICP-MS, EPMA, and Lubbers et al. (2022) trace element diffusion across plagioclase python script. Overall, in the past 1 Ma, the APMB magma chamber architecture below Cerro Uturuncu condensed while the magma itself became increasingly homogenous through convection mixing events. The magma was stored at or above plagioclase closure temperatures for under 1000 years prior to eruption for the youngest two of Cerro Uturuncu's lava stages.

DYNAMICS AND TIMESCALES OF MAGMATIC PROCESSES AT CERRO

UTURUNCU, BOLIVIA

By

Sarah Jane Rasor

A Master's Thesis
Submitted to the Graduate College
Of Missouri State University
In Partial Fulfillment of the Requirements
For the Degree of Master of Science, Geography and Geology

August 2023

Approved:

Gary Michelfelder, Ph.D., Thesis Committee Chair

Kevin Mickus, Ph.D., Committee Member

Mélida Gutiérrez, Ph.D., Committee Member

Julie Masterson, Ph.D., Dean of the Graduate College

ACKNOWLEDGEMENTS

I would also like to sincerely thank my family and friends for all their support from the moment they met me; my parents, Becky and John, sibling, Joseph, and honorary siblings, Oakley and Calypso, who have demonstrated unwavering support and love throughout all my ups and downs; my grandparents, LaVonne and Ralph Johnshoy and Joan Rasor, for creating a solid foundation for hard-working and loved generations and supporting me every moment for the past 24 years and onward; my amazing aunts, uncles, and cousins' support and laughs which motivate me to keep moving forwards. My friends, especially Kate Carpenter, who have made my life better no matter the distance between us; Ralph Harvey, of Case Western Reserve University, for believing in me no matter what and mentoring me throughout my time in university; and, my cat, Smokey, for making my world a million times better. From the moment I found Smokey here in Springfield, she has given me absolute, unparalleled joy. Smokey made Springfield bearable for me and really saved my life in general. I love you all. I couldn't be more grateful.

I dedicate this thesis to my family.

TABLE OF CONTENTS

LIST OF FIGURES

INTRODUCTION

Volcanoes are the surficial representation of magmatic dynamics and evolution over extensive periods of geologic time (Ginibre et al., 2007). In order to better understand volcanic events, we must first understand the source of these events (Ginibre et al., 2007). Midcrustal magma reservoirs have become recognized as an increasingly important source of magma storage and differentiation at continental arcs (Pritchard et al., 2018). However, there is a lack of understanding for irregular endmembers of continental arc volcanoes and their respective mid-crustal magma bodies (Michelfelder et al., 2014; Mamani et al., 2010; Kussmaul et al., 1977). In particular, within irregular continental arcs, stratovolcanoes' plumbing system evolutions are poorly constrained architecturally and geochemically (Viccaro et al., 2012). Fortunately, with the increase of success using plagioclase as an archive for magma plumbing evolution, we can contribute greater understanding to how stratovolcanic magma architecture develops throughout time (Ginibre et al., 2007, 2002; Costa et al., 2003).

The Central Andes are the type-endmember for thickest continental arcs (Pritchard et al., 2018). Through various seismology studies, it was determined that subduction between 12-25°S latitude occurs at approximately 30° (Tassara et al., 2006; Jordán et al., 1983). The continental crust composing the back arc area in the Andes, between 12-25°S latitude, reaches thicknesses of up to 75 kilometers, a thickness only subordinate to the Tibetan plateau, making it the thickest lithospheric subduction zone on the globe (Allmendinger et al., 1997). The height of the Andean orogeny and thickness of the underlying crust can be attributed to thin-skinned thrusts, lithospheric thickening from 12-10 Ma as a consequence of lithospheric cooling and shortening, as well as uplift beginning about 25 Ma (Scott et al., 2018; Mamani et al., 2010; Allmendinger et al., 1997; De Silva, 1989; Jordán et al., 1983). The regional magma

body in this area, the Altiplano Puna Magma Body (APMB), is the largest known mid-crustal magma body on the planet at an estimated 500,000 km^3 in volume (Pritchard et al., 2018; Ward et al., 2014; Zandt et al., 2003; Chmielowski et al., 1999). The unique attributes of the Central Andes warrant greater research.

Cerro Uturuncu is a Pleistocene composite volcano constructed above the center of the geophysical boundary of the APMB and thus provides valuable insight into the assimilation of continental crust into otherwise more mafic magma origins and the overall homogenization of the APMB (Michelfelder et al., 2014, 2013; Ward et al., 2014). Petrologic studies on Uturuncu have focused on whole-rock trace element geochemistry and petrogenesis separately from Uturuncu's relationship with the evolving APMB (Pritchard et al., 2018; Michelfelder et al., 2014, 2013). Previous studies have shown that Uturuncu lavas represent the homogenization of and concurrent crustal assimilation within the APMB (Michelfelder et al., 2014, 2013). However, it remains unclear how the homogenization affects the eruptive dynamics of Uturuncu and how residence times affect the actual homogeneity of the magma body. Integrating Uturuncu's whole-rock geochemistry and sub-crystal geochemistry with its central relationship to the APMB will provide much needed insight into the APMB's evolution over the past two million years, the APMB's inner plumbing, and Uturuncu's eruptive dynamics.

How the Altiplano-Puna Magma Body below Cerro Uturuncu evolves structurally and compositionally over time and the timescales at which magma resides within these magma chambers is still unknown. Through examining Uturuncu plagioclase chemistry and texture at the sub-crystal level and modeling trace element diffusion, we determine a clear picture of magma assembly, storage, and timescales within the APMB underneath Uturuncu. Trace element concentration, REE enrichment (relative to chondrites), major element concentration, and plagioclase textural analysis, was completed via laser ablation inductively coupled plasma

2

mass spectrometer (LA-ICP-MS), electron probe microanalyzer (EPMA), and optical microscopy. These analyses were used to determine the homogenization and evolution of magma chambers below Uturuncu over time. Employing the python script for trace element diffusion across plagioclase published by Lubbers et al. (2022) allowed us to constrain the brief timescales at which magma was stored in Cerro Uturuncu's more recent history.

GEOLOGIC SETTING

The stratovolcanic chain of the Central Andes is defined as the Andean Central Volcanic Zone (CVZ; Figure 1; de Silva, 1989; Francis and de Silva, 1989). The CVZ extends from 14-28°S, overrides up to 70 km of crust, and is characterized by large volume volcanism (Godoy et al., 2017; Ward et al. 2014; de Silva, 1989). The Altiplano-Puna Volcanic Complex (APVC) is found within the geologically defined boundary of the CVZ and is home to at least 20 calderas and large volcanic domes, and 50 active stratovolcanoes (Figure 1; Godoy et al., 2017; Michelfelder et al., 2013; de Silva, 1989). From 11-1 Ma, the APVC predominantly experienced expansive ignimbrite eruptions producing upwards of 15,000 km^3 of material (Pritchard et al., 2018; de Silva, 1989; Kussmaul et al., 1977). As a result, the stratovolcanoes within the APVC boundary, including Cerro Uturuncu, are constructed upon an extensive ignimbrite base, influencing much of the material erupted within the CVZ (Michelfelder et al., 2013; de Silva, 1989).

Below the APVC, is an underlying magmatic body called the Altiplano-Puna Magmatic Body (APMB; Figure 1; Pritchard et al., 2018; Ward et al., 2014; Chmielowski et al., 1999). The APMB is a mid-crustal magma body that begins approximately 15 km below sea-level and is centered under Cerro Uturuncu (Figure 1; Ward et al., 2014). Within the past few decades, the APMB has been observed through various seismology studies aiming to image the Central Andes at depth (Ward et al., 2014; Chmielowski et al., 1999). The extensive ignimbrite eruptions within the APVC have been linked to the APMB (Kern et al., 2016; de Silva et al., 2006). Correspondingly, APVC stratovolcanoes display petrochemical and compositional similarities to the underlying ignimbrites, suggesting magma generation occurs in the upper crust, where the low velocity zone is found (Ward et al., 2014; Fernandez et al., 1973).

While the petrochemical and geophysical data demonstrate upper crust partial melt, the area, however, is not homogeneously melted and mixed. The area of partial melt is estimated to be 500,000 km^3 in volume and between 4-25% melt, with the higher areas of melt increasing with proximity to the APMB center (Pritchard et al., 2018; Godoy et al., 2017; Ward et al., 2014; Chmielowski et al., 1999). Across the APVC, magma composition is only around 30% mantle-derived, which then incorporates upper crust within a mixing, assimilation, storage, and homogenization zone (MASH zone; Godoy et al., 2017; de Silva et al., 2006), with greater mantle derivation near the edges of the APMB, and more crustal assimilation toward its center (Godoy et al., 2017).

Cerro Uturuncu is a dormant Pleistocene stratovolcano in the CVZ within the boundary of the APVC and is potentially sourced by the APMB (Figure 1; Pritchard et al., 2018; Muir et al., 2015; Michelfelder et al., 2014; Sparks et al., 2008). Located in the southwest corner of Bolivia near the border of Chile and Argentina, Uturuncu is approximately 125 km behind the front arc of the CVZ (over 300 km inland from the Chilean coastline) which is an area volcanism is not typically seen within subduction zones (Figure 1; Michelfelder et al., 2014). Uturuncu is defined by six distinct andesitic to dacitic crystal-rich lava stages within recent geologic history (prior to 2 Ma; Muir et al., 2015; Michelfelder et al., 2014). Four of the recent stages are particularly voluminous: Puntas Negras (250-316 ka), Uturuncu (387-458 ka), Lomo Escapa (505-595 ka), and Cerro Agua de Pajarito (1016-1050 ka; Muir et al., 2015).

Cerro Uturuncu differs from the front-arc volcanoes in both location and eruptive compositions. Moho depths are approximately 35 km in the forearc and 70 km below the

plateaus (Yuan et al., 2002). Source magmas migrate through thicker crust under Uturuncu (~150 km) when compared to arc front volcanoes (~100 km; e.g. Aucanquilcha and Ollagüe) as evidenced by greater K_2O contents which indicate greater depth to the subducting slab (Figure 1; K-h relationship; Michelfelder et al., 2013; Feeley, 1993). Sr/Y ratios can be used as a proxy for crustal thickness and Moho depths (Lieu and Stern, 2019). Uturuncu has a relatively low Sr/Y ratio, suggesting that the magma source occurs in a plagioclase-stable, garnet-free environment (Lieu and Stern, 2019; Michelfelder et al., 2013). Furthermore, Uturuncu lavas have higher $^{87}Sr/^{86}Sr$ ratios than front arc lavas, suggesting that crustal contamination is much more significant near the center of the APMB and/or the lavas have differing source magmas (Godoy et al., 2017; Michelfelder et al., 2014, 2013; Feeley, 1993).

METHODS

Previously collected Uturuncu samples representing four volcanic stages suggested by Muir et al (2015) have been analyzed for $^{40}Ar/^{39}Ar$ ages, whole rock major and trace element contents, whole rock and plagioclase $^{87}Sr/^{86}Sr$ ratios, and oxygen isotope values (Muir et al., 2015; Michelfelder et al., 2014, 2013). Eight of the Uturuncu samples were chosen for in-depth sub- crystal analysis. Samples chosen for in-depth sub-crystal analysis are the following: UTUGSM53, UTDM106, UTDM37, UTDM90, UTUGSM69, UTDM63, UTUGSM18, and UTDM112. Muir (2015, 2014) renamed the samples to only "DM" or "GSM" for brevity. Based on whole rock geochemistry, these samples are either representative of a given lava stage or vastly differ from the representative geochemistry. Four of the samples are from the Puntas Negras stage (UTUGSM53, 250 ka; UTDM106, 268 ka; UTDM37, 280 ka; UTDM90, 282 ka), two from the Uturuncu stage (UTUGSM69, 387 ka; UTDM63, 455 ka), one from the Lomo Escapa stage (UTUGSM18, 501 ka), and one from the Cerro Agua de Pajarito stage (UTDM112, 1001 ka; Muir et al., 2015, 2014).

Textural Analysis

All plagioclase phenocrysts were texturally classified using optical microscopy. The optical microscope used for determining textures was the Leica DM750P microscope. Textures of interest include sieving, resorption surfaces, and spongey cores.

Plagioclase Major Element Analysis

For each Cerro Uturuncu sample (UTUGSM53, UTDM106, UTDM37, UTDM90, UTUGSM69, UTDM63, UTUGSM18, UTDM112), 10 to 15 plagioclase phenocrysts were

selected for major element analysis via electron microprobe at the University of Iowa and were combined with previously collected data by Michelfelder et al (2014). Major elements in plagioclase were analyzed using a JEOL JXA-8230 Superprobe (EPMA) with 5 wavelength-dispersive spectrometers and 8 large-format diffracting crystals based on the methodology described in Buckley (2022). Backscatter electron (BSE) images were taken to help identify plagioclase textures and zoning. Line transects were plotted from core to rim on each selected plagioclase phenocryst. The EPMA was programmed to take a 1 μm spot every 10 μm along the transect line from plagioclase core-to-rim. Each spot had a 4.25 minute run-time with a 15-30 second peak dwell time and a 5 second background dwell time. Analyses were conducted at an accelerating voltage of 15 keV with a 20 nA current. Major elements for the plagioclase phenocrysts were calibrated using the Astimex plagioclase, Cr-pyrope, and Orthoclase, and University of Iowa albite and anorthite standards. [43]Ca concentrations for plagioclase phenocrysts were used to determine molar anorthite percentage (X_{An}) and as an internal standard for completing the plagioclase trace element analysis.

Plagioclase Trace Element Analysis

For each Uturuncu sample (UTDM37, UTUGSM53, UTDM106, UTDM90, UTUGSM69, UTDM63, UTUGSM18, UTDM112), the same 10 to 15 plagioclase phenocrysts selected for major element analysis were chosen for an in-depth trace element analysis. Plagioclase phenocrysts were chosen based on the presence of zoning in XPL optical microscopy, minimal cracks and inclusions, representation of other plagioclase phenocrysts present in the sample, and adequate size of phenocrysts for analysis. The laser ablation inductively coupled mass spectrometer (LA-ICP-MS) was chosen for minor and trace element analysis as it has the needed resolution, detection limits, and allows for rapid analysis (Ginibre

et al., 2007; Davidson et al., 2001, 1999). Analysis of plagioclase minor and trace elements was conducted at the University of Arkansas Trace Element and Radiogenic Isotope Lab using LA- ICP-MS. The LA-ICP-MS used is an ESI NWR 193 nm Excimer Laser Ablation System coupled with a Thermo Scientific iCapQ Quadrupole Mass Spectrometer. The following elements were analyzed for each plagioclase phenocryst: Li, Mg, Si, Sc, Ti, Cr, Fe, Zn, Rb, Sr, Y, Zr, Nb, Cs, Ba, La, Ce, Pr, Nd, Sm, Eu, Gd, Tb, Dy, Ho, Er, Tm, Yb, Lu, Hf, Pb, Th, and U. Elements were selected based on natural occurrence, isotopic occurrence, and lack of isobaric, doubly charged, and polyatomic interferences. Elements were selected based on their ability to comment on plagioclase populations, source magmas, mixing, and homogenization.

Each plagioclase phenocryst was analyzed by the LA-ICP-MS in two ways. First, by ablating 50 µm wide transect lines from core-to-rim and, second, by 50 µm diameter spots paralleling the transect. Sample UTDM37 was only analyzed with spot analysis. Line transects were scanned at 10 µm/sec. The use of transect lines with corresponding adjacent points was selected for greater data resolution for plagioclase core-to-rim transects. Statistical analysis has demonstrated that plagioclase zones grow perpendicular to the A and B axes of the crystal and are perpendicular to crystal boundaries no matter how unideal the thin section (Cheng et al., 2017). Though it is worth noting that off-center sections can affect the appearance of plagioclase populations (Cheng et al., 2017). Depending on the size of the plagioclase phenocryst, 1 to 2 transect lines were analyzed from core-to-rim. Similarly, parallel each transect, 2-7 spots were analyzed from core-to-rim. The plagioclase phenocryst spots are classified by the spot in the center of the phenocryst, on the rim of the phenocryst, and all the spots between them, which are referred to as the "core," "rim," and "mantle," respectively.

LA-ICP-MS data was reduced using the Iolite 4 software package using both NIST610 and NIST612 as external standards (Paton et al., 2011; Woodhead et al., 2007). Plagioclase

phenocryst ^{43}Ca values collected with the EPMA were input as the calibration isotope within Iolite. Rare earth elements (La, Ce, Pr, Nd, Sm, Eu, Gd, Tb, Dy, Ho, Er, Tm, Yb, and Lu) were normalized to chondrite values defined by McDonough and Sun (1995).

Diffusion Modeling

Elemental diffusion defines a crystal's residence time within the magma chamber and how much time the crystal was held at or above the closure temperature (Davidson et al., 2001; Zellmer et al., 1999). Representative plagioclase phenocrysts with known spatial chemical composition have been shown to be useful in determining residence times within the magma plumbing system (Lubbers et al., 2022; Chen et al., 2020; Davidson et al., 2007; Costa et al., 2003; Ginibre et al., 2002; Francalanci et al., 1999; Zellmer et al., 1999; Cherniak and Watson, 1994; Albarède, 1993). Strontium is compatible with plagioclase in the upper crust, making Sr concentrations across crystal zones significant for determining residence times through diffusion modeling (Davidson et al., 2008, 2007; Ginibre et al., 2007; Francalanci et al., 1999; Davidson and Tepley, 1997; Albarède, 1993).

Approximately 10 to 15 plagioclase phenocrysts in four of the five most recent samples (UTUGSM53, UTDM106, UTDM90, and UTUGSM69) were selected for Sr diffusion modeling. To model trace element diffusion across plagioclase zones, we implemented the python script provided by Lubbers et al. (2022). The inputs for plagioclase diffusion model are temperature and trace element concentration (Sr, Mg, Na; dependent on timescale; Lubbers et al., 2022). Based on Uturuncu Zircon temperatures, we use 770C as the temperature input. Similarly, given the APMB's upper-crustal origins and Uturuncu zircon ages, Sr was selected for the trace element to be diffusion modeled. Consequently, spatially defined Sr and X_{An} collected by the LA-ICP-MS and EPMA, respectively, are also inputs. Molar Anorthite data is

10

a necessary input as the diffusion coefficient for trace elements in plagioclase differs with X_{An} (Tepley et al., 2010, 2000, 1999; Costa et al., 2003; Zellmer et al., 1999; Cherniak and Watson, 1994; Giletti and Casserly, 1994). Partition coefficient and trace element diffusion coefficient are determined based on the experimental paper Bindeman et al. (1998) and the previously stated inputs. Overall, the code from Lubbers et al. (2022) uses the diffusion equation determined in Costa et al. (2003) to model the diffusion of Sr. Final residence age results are produced through the Monte Carlo method.

Plagioclase Petrography

Thin section descriptions for UTDM37, UTUGSM53, UTDM106, UTDM90, UTUGSM69, UTDM63, UTUGSM18, UTDM112 are presented in detail by Michelfelder et al. (2014) and Muir et al. (2015, 2014). The following phases are present in all thin sections: plagioclase, orthopyroxene, biotite, Fe-Ti oxides, and glass (Michelfelder et al., 2014). Minor phases include quartz, clinopyroxene, hornblende, zircon, and monazite, which are only present in some of the thin sections (Michelfelder et al., 2014).

Plagioclase phenocrysts were first classified texturally to establish distinct plagioclase populations. Across all samples, notable textures include spongy cores, sieving at the rims, resorption surfaces, and synneusis (also noted in Muir et al., 2014; Figure 2). Both the presence of and the amount of these texture types were considered. Puntas Negras stage plagioclase nearly all exhibited spongy cores and synneusis while about half had sieved rims and fine zoning. Only a few plagioclase phenocrysts in this stage have resorption surfaces. Similarly, nearly all of Uturuncu stage plagioclase were also observed to have spongy cores while, unlike Puntas Negras, few plagioclase phenocrysts have sieved rims. Half of plagioclase in the Uturuncu stage displayed fine zoning while resorption surfaces were rarely seen. About two-thirds of Uturuncu stage plagioclase displayed synneusis. Almost all of Lomo Escapa plagioclase had observed spongy cores and sieved rims. Differing from the earlier two stages, Lomo Escapa plagioclase displayed few crystals with synneusis. A minority of crystals in the Lomo Escapa stage had fine zoning and resorption surfaces. Similar to Lomo Escapa plagioclase, Cerro Agua de Pajarito stage plagioclase nearly always exhibited spongy cores and sieved rims. Cerro Agua de Pajarito plagioclase had more instances of synneusis than Lomo

Escapa but still much less than the earliest stages. About half of the plagioclase in Cerro Agua de Pajarito had resorption surfaces and fine zoning. Spongy cores were seen most extensively in plagioclase phenocrysts that were relatively large (>500 μm) with considerable zoning across all stages.

Major Element Chemistry

Molar percent anorthite (X_{An}) across plagioclase zones was determined for Puntas Negras stage samples UTUGSM53, UTDM106, and UTDM90, and Uturuncu stage sample UTUGSM69. Overall, Puntas Negras samples had a greater X_{An} spread which ranged from An_{47-94} with an average of An_{67}. Individually, UTUGSM53 plagioclase zones had a range from An_{51-93} with an average of An_{66}; UTDM106 plagioclase zones had a range from An_{47-94} with an average of An_{66}; and, UTDM90 plagioclase zones had a range from An_{60-83} with an average of An_{68}. Uturuncu sample UTUGSM69 plagioclase zones had a lower and narrower range from An_{54-80} with an average of An_{64}. There were slight positive trends between Puntas Negras and Uturuncu plagioclase MgO weight percent (wt%) and X_{An} (Figure 3). This slight positive trend can also be seen between FeO wt% and X_{An} (Figure 3).

The pattern of which the plagioclase has experienced varying X_{An} is referred to as the zoning pattern (Ginibre et al., 2007). Types of zoning patterns include "normal," "reverse," "oscillatory," and "patchy" as defined by Ginibre et al. (2007). Molar Anorthite percentage variations across individual plagioclase' zones for UTUGSM53, UTDM106, UTDM90, and UTUGSM69 indicate that magma with eruption ages between 387-250 ka can be characterized by oscillatory zoning and monotonous normal zoning, with a small amount of plagioclase displaying reverse zoning.

Plagioclase trace element data collected with the LA-ICP-MS is illustrated in Figure 4

(separate graphs in Appendices A and B). Cerro Uturuncu plagioclase Fe values range from 680±40 to 11407±1968 ppm. Iron concentration range increases in breadth as the stages decrease in age: Puntas Negras (316-250 ka) from 680±40 to 11407±1968 ppm; Uturuncu (458-387 ka) from 708±23 to 7542±292 ppm; Lomo Escapa (595-505 ka) from 1296±34 to 10053±1217 ppm; Cerro Agua de Pajarito (1050-1018 ka) from 1670±55 to 7439±239 ppm (Figure 4).

Trace Element Chemistry

Lithium, Mg, Sr, and Ba were plotted against Fe for each sample (Figure 4). Cerro Uturuncu plagioclase Li concentration ranges from 17.3±0.998 to 153±5.15 ppm; Mg concentration ranges from 54.0±1.90 to 1332±135 ppm; Sr concentration ranges from 379±9.07 to 2710±60.7 ppm; and, Ba concentration ranges from 47.9±1.43 to 1185±27.0 ppm (Figure 4). Ranges of values for each trace element are very similar across stages, however, concentration clustering varies (Figure 4; Appendices A and B). Puntas Negras stage Li concentration ranges from 22.4±1.41 to 137±3.07 ppm; Mg concentration ranges from 54.0±1.90 to 1332±135 ppm; Sr concentration ranges from 379±9.07 to 2710±60.7 ppm; Ba concentration ranges from 79.4±3.34 to 1185±27.0 ppm (Figure 4; Appendix A). Puntas Negras stage Li, Mg, Sr, and Ba contents each display two to three distinct clusters of concentration (Appendix A). It is worth noting that Puntas Negras consistently has the widest range of trace element concentration variation for Fe, Li, Mg, Sr, and Ba compared to the other stages. Uturuncu stage Li concentration ranges from 20.1±1.24 to 114±4.20 ppm; Mg concentration ranges from 60.0±1.99 to 621±59.3 ppm; Sr concentration ranges from 799±15.4 to 2360±47.8 ppm; and, Ba concentration ranges from 49.1±2.07 to 838±30.1 ppm (Figure 4; Appendix A). Uturuncu stage Li, Mg, Sr, and Ba contents each display two to three distinct clusters of concentration

(Appendix A). Lomo Escapa stage Li concentration ranges from 51.7±2.15 to 153±5.15 ppm; Mg concentration ranges from 62.2±1.68 to 811±45.9 ppm; Sr concentration ranges from 1233±24.8 to 2599±56.1 ppm; and, Ba concentration ranges from 47.9±1.43 to 682±19.0 ppm (Figure 4; Appendix B). Lomo Escapa stage Li, Mg, Sr, and Ba contents each demonstrate one distinct cluster of concentration, though are relatively varied overall (Appendix B). Lastly, Cerro Agua de Pajarito stage Li concentration ranges from 17.3±0.998 to 128±17.1 ppm; Mg concentration ranges from 139±4.04 to 969±112 ppm; Sr concentration ranges from 847±16.3 to 1899±38.4 ppm; and, Ba concentration ranges from 66.3±2.10 to 1045±46.4 ppm (Figure 4; Appendix B). Cerro Agua de Pajarito stage Li, Mg, Sr, and Ba contents do not demonstrate any notable concentration clustering (Appendix B). Across all stages, rims and mantles tend to have the largest concentration of Li, Mg, Sr, and Ba, while rims alone have the greatest concentration of Fe (Figure 4; Appendices A and B).

Rare earth element (REE) data is illustrated in Figure 5-9. Overall, Cerro Uturuncu plagioclase has a wide variation in REE enrichment relative to chondrites with La ranging from 11.0 to 471 with an average of 170, Lu ranging from 0.0482 to 8.12 with an average of 0.583, Eu/Eu* ranging from 2.62 to 20.8 with an average of 8.90, La/Dy ranging from 15.8 to 358 with an average of 75.3, La/Sm ranging from 4.28 to 17.0 with an average of 9.26, and Dy/Dy* ranging from 0.168 to 5.13 with an average of 1.02. Puntas Negras and Cerro Agua de Pajarito both display an extensive range in REE values while Uturuncu and Lomo Escapa demonstrate a much narrower range (Figure 5). Ranges of REE enrichment relative to chondrites within Puntas Negras include Lu from 16.4 to 471 with an average of 178, Lu from 0.0482 to 8.13 with an average of 0.547, Eu/Eu* from 2.62 to 18.5 with an average of 8.86, La/Dy 19.5 to 259 with an average of 74.9, La/Sm from 5.85 to 17.0 with an average of 9.37, and Dy/Dy* from 0.252 to 5.13 with an average of 1.03 (Figure 6). Samples within Puntas Negras Stage

(UTUGSM53, UTDM106, UTDM37, UTDM90) display one to two homogenous groups of REE enrichment; UTDM106 and UTUGSM53 have one group of REE enrichment while, UTDM37 and UTDM90 demonstrate two (Figure 6). Overall, Puntas Negras plagioclase have two distinct groups of REE enrichment. Most individual plagioclase within Puntas Negras have homogenous REE enrichment from core to rim, though some plagioclase phenocrysts exhibit greater REE enrichment at the rim (Figure 8). Uturuncu Stage (UTUGSM69, UTDM63) plagioclase are mostly homogenous with high LREE/HREE ratios and pronounced positive Eu anomalies (Figure 7). Uturuncu Stage plagioclase have enrichment relative to chondrites in La ranging from 76.9 to 363 ppm with an average of 170 ppm, Lu ranging from 0.0576 to 5.37 with an average of 0.568, Eu/Eu* ranging from 3.49 to 18.1 with an average of 9.00, La/Dy ranging from 31.5 to 307 with an average of 82.1, La/Sm from 6.08 to 16.9 with an average of 9.49, and Dy/Dy* ranging from 0.168 to 2.75 with an average of 1.04 (Figure 7). Lomo Escapa (UTUGSM18) is slightly more variable than Uturuncu stage plagioclase, though very similar overall (Figure 5). Many Lomo Escapa plagioclase demonstrate low, positive Eu anomalies as well (Figures 5 and 7). Cores, mantles, and rims for Lomo Escapa are very homogenous (Figure 7). Some individual plagioclase phenocrysts exhibit an increase in REE values from core to rim (Figure 9). Ranges of REE enrichment relative to chondrites within Lomo Escapa (UTUGSM18) include Lu from 109 to 247 with an average of 163, Lu from 0.0689 to 4.99 with an average of 0.758, Eu/Eu* from 3.40 to 13.7 with an average of 9.16, La/Dy 15.8 to 358 with an average of 73.8, La/Sm from 4.28 to 15.2 with an average of 9.08, and Dy/Dy* from 0.571 to 2.07 with an average of 0.970 (Figure 7). Cerro Agua de Pajarito (UTDM112) plagioclase is extremely variable with a significantly wide range in LREE/HREE with many demonstrating low positive Eu anomalies (Figure 7). Rims tend to be more homogenous with greater amounts of REEs (Figure 9). Based on singular plagioclase phenocrysts, we see that

cores and mantles tend to be more homogenous while rims demonstrate vastly greater amounts of REEs (Figure 9). Cerro Agua de Pajarito stage plagioclase have enrichment relative to chondrites in La ranging from 11.0 to 319 ppm with an average of 113 ppm, Lu ranging from 0.0728 to 5.26 with an average of 0.791, Eu/Eu* ranging from 3.15 to 20.8 with an average of 8.43, La/Dy ranging from 19.5 to 114 with an average of 55.1, La/Sm from 5.32 to 10.5 with an average of 7.65, and Dy/Dy* ranging from 0.235 to 1.65 with an average of 0.819 (Figure 7). Line transect trace element concentration data collected from the LA-ICP-MS concurred with the spot analysis. Most notably, across all samples (UTDM37, UTUGSM53, UTDM106, UTDM90, UTUGSM69, UTDM63, UTUGSM18, and UTDM112) Sr and Ba concentrations mimic one another from core to rim on each plagioclase phenocryst (Figure 10). Mg and Fe concentrations also mimic one another from each core to rim transect (Figure 10).

DISCUSSION

Magma bodies fueling Cerro Uturuncu's eruption history have yet to be constrained chemically and structurally over the past 1 Ma. Magma assembly, storage, and timescales at Cerro Uturuncu are visualized through textural, major element, and trace element analysis. Using samples from four of the most recent lava stages in Uturuncu's history: Puntas Negras (316-250 ka), Uturuncu (458-387 ka), Lomo Escapa (595-505 ka), and Cerro Agua de Pajarito (1050-1016 ka)—the magma bodies' evolution over the past 1 Ma is reconstructed. Sub-plagioclase textures help explain magmatic processes and events that take place within Uturuncu magma chambers over time (Hughes et al., 2021; Renjith, 2014; Tepley et al., 2000). Similarly, sub-plagioclase chemistry captures compositional changes within Uturuncu magma bodies through its zonal growth (Ginibre et al., 2007, 2002). By combining sub- plagioclase qualitative and quantitative analyses with plagioclase residence times and eruption ages, a spatial and temporal evolution of Uturuncu magma bodies is proposed.

Plagioclase Petrography Interpretations

Plagioclase phenocryst textures also suggest many magma processes and events. Spongy cores, resorption surfaces, and sieved rims indicate disequilibrium within the magma chamber (Hughes et al., 2021; Renjith, 2014; Tepley et al., 2000). Synneusis also reflects magma chamber dynamics (Renjith, 2014). Spongy cores, also referred to as course sieving within the middle of the crystal, indicate decompression melting (Figure 2; Renjith, 2014). The resorption surfaces suggest that the plagioclase experienced extensive dissolution with the introduction of parental magma and consequential interaction over an extended period of time (Figure 2; Renjith, 2014; Tepley et al., 2000). The fine sieving observed at the plagioclase rims illustrates

the dissolution of the plagioclase as it reacts with hotter, more Ca-rich magma (Figure 2; Renjith, 2014). Additionally, as the sieving is widely seen at the plagioclase rims, it is likely that there was an influx of hot, Ca-rich magma just prior to eruption, potentially acting as an initiator (Figure 2; Davidson et al., 2007, 1999; Ginibre et al., 2007, 2002). Synneusis can be attributed to convection throughout the magma chamber (Figure 2; Renjith, 2014). As a vast majority of plagioclase in the Puntas Negras stage demonstrate spongy cores and synneusis, the magma chambers fueling this stage experienced decompression melting and consistent convection throughout (Renjith, 2014). With around half of the plagioclase with sieved rims, hotter, Ca-rich magma was introduced to the magma plumbing system in the Puntas Negras stage (Renjith, 2014; Ginibre et al., 2007). There was likely few to no extended interactions between plagioclase and parental magma in the Puntas Negras stage as few phenocrysts exhibited resorption surfaces (Renjith, 2014). Similar to Puntas Negras, a majority of Uturuncu stage plagioclase had spongy cores and synneusis suggesting that decompression melting and chamber convection were also major magma chamber dynamics in this stage (Renjith, 2014). There was also likely few to no extended interactions between plagioclase and parental magma in the Uturuncu stage as very few phenocrysts exhibited resorption surfaces (Renjith, 2014). However, as few plagioclase phenocrysts have sieved rims, the introduction of hotter, Ca-rich magma in the Uturuncu stage was rare (Renjith, 2014; Ginibre et al., 2007). Decompression melting and the introduction of hotter, Ca-rich magma was very prevalent in the Lomo Escapa stage as almost all plagioclase had observed spongy cores and sieved rims (Renjith, 2014; Ginibre et al., 2007). Differing from the earlier two stages, Lomo Escapa plagioclase displayed few phenocrysts with synneusis suggesting that convection throughout the chamber was not occurring as extensively (Renjith, 2014). Additionally, as resorption surfaces were not highly prevalent, likely few to no extended interactions between plagioclase and parental magma

occurred in the Lomo Escapa stage either (Renjith, 2014). Similar to Lomo Escapa plagioclase, Cerro Agua de Pajarito stage plagioclase nearly always exhibited spongy cores and sieved rims emphasizing the pervasiveness of decompression melting and the introduction of hotter, Ca-rich magma (Renjith, 2014; Ginibre et al., 2007). Cerro Agua de Pajarito plagioclase had more instances of synneusis than Lomo Escapa but still much less than the earliest stages which demonstrates that, though convection throughout the chambers was occurring, it occurred less than in the earliest two stages (Renjith, 2014). Finally, with resorption surfaces observed in half of the plagioclase, extended interactions between plagioclase and parental magma occurred in Cerro Agua de Pajarito stage magma chambers (Renjith, 2014). Overall, the younger stages experienced greater convection throughout the magma bodies than the older stages; magma interactions shifted from prolonged interactions with parental magma to increasingly fewer short reactions with hotter, Ca-rich magma as the magma chambers evolved. As the fine-scale sieving occurred at the plagioclase rims, it is likely that, for all stages, the introduction of hotter, Ca-rich magma contributed to the pending eruptions (Davidson et al., 2007, 1999; Ginibre et al., 2007, 2002). All stages experienced decompression melting.

Major Element Chemistry Interpretations

Changes in molar anorthite percentage (X_{An}) demonstrates the thermal and compositional evolution the plagioclase experienced over time (Ginibre et al., 2007). Puntas Negras and Uturuncu (UTUGSM53, UTDM106, UTDM90, and UTUGSM69) plagioclase can be characterized by oscillatory zoning and monotonous normal zoning, with a small amount of reverse zoning, the implications are as follows: oscillatory zoning suggests that the magma was consistently oscillating in temperature—likely caused by small-scale convection—to produce the X_{An} highs and lows within the plagioclase zones (Renjith, 2014; Davidson et al., 2007;

Ginibre et al., 2007); monotonous normal zoning likely precipitated during a single oscillatory period as the chamber gradually cools after a heating event (Davidson et al., 2007; Ginibre et al., 2007). The relative highs in temperature can be attributed to an influx of new magma and/or magma mixing as there was no significant correlation between changes in MgO or FeO wt% and X_{An} (Figure 3; Davidson et al., 2007).

Trace Element Chemistry Interpretations

Trace element concentrations were also used to distinguish and group plagioclase phenocrysts (Davidson et al., 2007, 1999; Ginibre et al., 2007, 2002). Puntas Negras and Uturuncu stage plagioclase tend to have two distinct clusters of trace element compositions; Lomo Escapa stage has one distinct cluster of trace element composition though trace element data is variable overall; and, Cerro Agua de Pajarito stage plagioclase have variable trace element compositions with no notable clustering. The variability of trace elements becoming distinctly homogeneous within the younger lavas demonstrates that the underlying plumbing system was likely numerous small heterogeneous bodies of partial melt during the Cerro Agua de Pajarito (1050-1016 ka) and Lomo Escapa stages (595-505 ka; Figure 11). During the Lomo Escapa stage, eruptions were primarily fueled by one chamber as evidenced by a singular cluster of trace element composition within a varied spread (Figure 11).

Overall, Cerro Agua de Pajarito (1050-1016 ka) and Lomo Escapa (595-505 ka) were fed by numerous small magma bodies (Figure 11). As the plumbing system evolved, magma injections and consequential increased volume of the magma bodies led to the consolidation of the smaller chambers (Figure 11). By the Uturuncu (458-387) and Puntas Negras stages (316-250 ka), the underlying magma plumbing system had evolved to be two to three larger bodies of partial melt (Figure 11). The bodies fueling Uturuncu and Puntas Negras stages were

distinctly homogeneous through thorough magma mixing indicated by the tight, distinct trace element concentrations (Figure 11).

Rare earth elements demonstrate varying enrichment patterns and corresponding fractional crystallization (Lubbers et al., 2022; Boynton et al., 2013; Michelfelder et al., 2013). Varying REE enrichment across plagioclase cores, mantles, and rims suggest different growth histories with diverse degrees of enrichment (Boynton et al., 2013). REE data corroborates the assertion that multiple small magma chambers evolved into few larger and more homogenous bodies as Cerro Agua de Pajarito plagioclase have very variable REE concentrations with no distinct plagioclase populations (Figures 5 and 11). Magma fueling Cerro Agua de Pajarito was coming from many chemically dissimilar chambers (Figure 11). REE enrichment increases at Cerro Agua de Pajarito plagioclase rims suggesting fractional crystallization was occurring within the chambers between 1016-1050 ka (Figures 8, 9, and 11; Boynton et al., 2013). Lomo Escapa plagioclase REE enrichment was homogenous, suggesting that one of the many chambers primarily fueled volcanism during this period (Figures 7 and 11). REE enrichment increases at plagioclase rims suggesting fractional crystallization was taking place during the Lomo Escapa stage plagioclase growth as well (505-595 ka; Figure 9; Boynton et al., 2013). Uturuncu stage plagioclase display one population of REE enrichment suggesting one homogenous chamber fueled the eruptions between 387-458 ka (Figures 7 and 11). There is a slight increase in REE enrichment at Uturuncu stage plagioclase rims suggesting that fractional crystallization was occurring (Figure 9; Boynton et al., 2013). Puntas Negras has two distinct REE plagioclase populations suggesting two homogenous magma bodies fueled the eruptions between 250-316 ka (Figures 6 and 11). Fractional crystallization is not extensively occurring in the Puntas Negras stage as there is no pronounced REE enrichment at the rim of the plagioclase (Figure 8; Boynton et al., 2013). As the increase in REE enrichment is less than

what is seen in the older stages, the fractional crystallization was not as extensive between 458-250 ka as it was between 1050-505 ka (Boynton et al., 2013).

Plagioclase Populations

Sub-plagioclase geochemical analyses and textural observations illuminate the evolutionary history of the plumbing system below Cerro Uturuncu. Plagioclase populations for the four stages allows for the constraint of individual magma chambers within the system. Plagioclase populations share a common history, or part of it, identified by common characteristics within zones (Ginibre et al., 2002). In that way, plagioclase populations can illustrate the different locales within magma bodies and events changing magma composition below the volcano (Hughes et al., 2021). Individual plagioclase populations were established by texture, major element concentration and zoning pattern, and trace element concentrations and corresponding REE enrichment.

Overall, Puntas Negras (316-250 ka) characterized by two distinctly homogeneous plagioclase populations; Uturuncu (458-387 ka) by one distinctly homogenous population; Lomo Escapa (595-505 ka) by various plagioclase populations (one distinct and other heterogeneous populations); and, Cerro Agua de Pajarito (1050-1018 ka) by many heterogeneous plagioclase populations. Consequently, the magma architecture below Cerro Uturuncu evolved from many heterogeneous chambers to larger homogeneous bodies over Cerro Uturuncu's eruptive history (Figure 11). The increased homogeneity can be attributed to more thorough mixing within the chambers between 458-250 ka as evidenced by a much greater presence of synneusis textures indicating extensive conduction within the magma bodies. More prevalent resorption surfaces and sieved rims in the older stages (1050-505 ka) also impacted the heterogeneity of those stages as parental and hotter, Ca-rich magma was

more commonly introduced. Once those magmatic compositionally end members were mixed

into the existing magma thoroughly, the composition of the magma bodies became more

compositionally homogenous between 458-250 ka.

Diffusion Modeling Timescales

Approximately 10 to 15 plagioclase phenocrysts in four of the five most recent samples

(UTUGSM53, UTDM106, UTDM90, and UTUGSM69) were selected for Sr diffusion

modeling using the diffusion modeling code published by Lubbers et al. (2022). Results

indicate that average residence times are 1488.8 years for UTUGSM53, 351.5 years for

UTDM106, 220.7 years for UTDM90, and 203.3 years for UTUGSM69 (Figure 12).

Consequently, the average residence time for Puntas Negras stage is 721.3 years while

Uturuncu stage is 203.3 years. For geologic timescales, these residence times are relatively

short. Magma residence time and eruption ages are shown in Figure 12. Two sigma values are

large for the modeled residence times and many models showed skewed distributions

suggesting that further work must be completed to generate more accurate models (Figure 12).

Connection to the APMB

Uturuncu's magma plumbing system can be further connected to the Altiplano-Puna

Magma Body (APMB). The resolution of geophysical studies cannot visualize the facets of the

plumbing system, but rather the overarching area of the APMB (Ward et al., 2014). However,

previous research conducted by Muir et al. (2014) and Hickey et al. (2013) has suggested that

Cerro Uturuncu is fueled from the depth at which the APMB resides, indicating that the APMB

is the source of Cerro Uturuncu eruptions. Determining the magma plumbing architecture

Cerro Uturuncu sources for eruptions, therefore, visualizes the APMB structure below Cerro

Uturuncu (Muir et al., 2014; Hickey et al., 2013). Thus, the interpretations of Cerro Uturuncu's plumbing system discussed in detail above are interpretations of the APMB. From 1050-250 ka, the APMB has become structurally condensed and chemically homogenous below Cerro Uturuncu.

CONCLUSION

The use of sub-crystal analysis of plagioclase helped visualize the evolution of the magma chamber architecture below Cerro Uturuncu over its eruptive history. Optical textures, major element, and trace element chemistry allowed for detailed plagioclase growth history evaluation. Plagioclase textures (spongy cores, fine zoning, and sieved rims) suggests new magma influxes and mixing events caused chemical and temperature fluctuations and corresponding disequilibrium. Synneusis also indicated an increase in convection within the magma bodies overtime. Overall, the APMB plumbing system below Cerro Uturuncu has experienced chamber consolidation and homogenization. From 1001 to 250 ka, the magma structure shifted from many compositionally diverse isolated chambers to a few compositionally homogeneous chambers. This evolution of the magma plumbing architecture is evidenced by changing trace element clustering and REE enrichment across four of Cerro Uturuncu's eruptive stages. Puntas Negras (316-250 ka) demonstrated two distinctly homogeneous plagioclase populations through trace element and REE analysis. Each individual sample within Puntas Negras stage had one to two of those plagioclase populations suggesting that the two chambers erupting did not always do so at the same time. Uturuncu (458-387 ka) could also be characterized by two plagioclase populations. These populations erupted from two chambers that were well-mixed and distinctly homogeneous. Lomo Escapa (595-505 ka) had one distinct plagioclase population, though plagioclase was varied overall. During the Lomo Escapa stage, there were many poorly-mixed magma chambers. It is likely that, because there is one distinct plagioclase population, material was mainly erupted from one chamber. Cerro Agua de Pajarito (1050-1018 ka) had no distinct plagioclase populations and displayed widely varied trace element concentrations and REE enrichment. Material from the

26

Cerro Agua de Pajarito stage erupted from many unevolved and poorly-mixed, heterogenous chambers. Fractional crystallization occurred throughout Cerro Uturuncu's history, though it became less extensive in younger lava stages. Magma was stored for relatively short periods of time prior to eruption. Diffusion modeling of Sr across plagioclase zones suggests that Puntas Negras Stage plagioclase resided in magma chambers on average for approximately 721.3 years prior to eruption while Uturuncu stage plagioclase resided in the chamber on average for about 203.3 years prior to eruption. However, given the extensivity of spongy cores, resorption surfaces, and sieved rims, the plagioclase spent additional time within the chamber under conditions not conducive of crystal growth.

REFERENCES

Albarède, F., 1993, Residence time analysis of geochemical fluctuations in volcanic series: Geochimica et Cosmochimica Acta, v. 57, p. 615-621, https://doi.org/10.1016/0016- 7037(93)90372-4.

Allmendinger, R.W., Jordan, T.E., Kay, S.M., and Isacks, B.L., 1997, The evolution of the Altiplano-Puna plateau of the Central Andes: Annual review of earth and planetary sciences, v. 25, p. 139-174, https://doi.org/10.1146/annurev.earth.25.1.139.

Bindeman, I.N., Davis, A.M. and Drake, M.J., 1998, Ion microprobe study of plagioclase-basalt partition experiments at natural concentration levels of trace elements: Geochimica et Cosmochimica Acta, v. 62, p.1175-1193, https://doi.org/10.1016/S0016-7037(98)00047-7.

Boynton, W.V., Clark, A.M., Cullers, R.L., Fleet, A.J., Frey, F.A., Graf, J.L., Haskin, L.A., Hawkesworth, C.J., Henderson, P., Highly, D.E., Humphris, S.E., Neary, C.R., Pankhurst, R.J., Saunders, A.D., and van Calsteren, P.W.C., 2013, Rare earth element geochemistry: Elsevier Science, 510 p.

Buckley, K.L., 2022, Aucanquilcha Volcanic Cluster Magma Evolution and Magma Plumbing System Architecture During the Gordo Stage (6-4 Ma) [M.Sc. Thesis]: Missouri State University, 261 p.

Chen, Z., Zeng, Z., Wang, X., Peng, X., Zhang, Y., Yin, X., Chen, S., Zhang, L., and Qi, H., 2020, Element and Sr isotope zoning in plagioclase in the dacites from the southwestern Okinawa Trough: insights into magma mixing processes and time scales: Lithos, v. 376, p. 105776, https://doi.org/10.1016/j.lithos.2020.105776.

Cheng, L., Costa, F. and Carniel, R., 2017, Unraveling the presence of multiple plagioclase populations and identification of representative two-dimensional sections using a statistical and numerical approach: American Mineralogist: Journal of Earth and Planetary Materials, v. 102(9), p.1894-1905, https://doi.org/10.2138/am-2017-5929CCBYNCND.

Cherniak, D.J., and Watson, E.B., 1994, A study of strontium diffusion in plagioclase using Rutherford backscattering spectroscopy: Geochimica et Cosmochimica Acta, v. 58, p.5179-5190, https://doi.org/10.1016/0016-7037(94)90303-4.

Chmielowski, J., Zandt, G., and Haberland, C., 1999, The central Andean Altiplano-Puna magma body: Geophysical Research Letters, v. 26, p. 783-786, https://doi.org/10.1029/1999GL900078.

Costa, F., Chakraborty, S., and Dohmen, R., 2003, Diffusion Coupling between Trace and Major Elements and a Model for Calculation of Magma Residence Times Using Plagioclase: Geochimica Et Cosmochimica Acta, v. 67, p. 2189–2200, https://doi.org/10.1016/s0016-7037(02)01345-5.

Davidson, J.P., Font, L., Charlier, B.L., and Tepley, F.J., 2008, Mineral-scale Sr isotope variation in plutonic rocks—a tool for unravelling the evolution of magma systems: Earth and Environmental Science Transactions of the Royal Society of Edinburgh, v. 97, p. 357-367, https://doi.org/10.1017/S0263593300001504.

Davidson, J.P., Morgan, D.J., and Charlier, B.L., 2007, Isotopic microsampling of magmatic rocks: Elements, v. 3, p. 253-259, https://doi.org/10.2113/gselements.3.4.253.

Davidson, J.P., Morgan, D.J., Charlier, B.L.A., Harlou, R., and Hora, J.M., 2007, Microsampling and isotopic analysis of igneous rocks: implications for the study of magmatic systems: Annu. Rev. Earth Planet. Sci., v. 35, p. 273-311, https://doi.org/10.1146/annurev.earth.35.031306.140211.

Davidson, J., Tepley III, F., Palacz, Z., and Meffan-Main, S., 2001, Magma recharge, contamination and residence times revealed by in situ laser ablation isotopic analysis of feldspar in volcanic rocks: Earth and Planetary Science Letters, v. 184, p. 427-442, https://doi.org/10.1016/S0012-821X(00)00333-2.

Davidson, J.P., Tepley III, F.J., Palacz, Z. and Meffan-Main, S., 1999, August. Crystal Isotopic Stratigraphy Using Laser Ablation: In Ninth Annual VM Goldschmidt Conference, p. 7141.

Davidson, J.P. and Tepley III, F.J., 1997, Recharge in volcanic systems: evidence from isotope profiles of phenocrysts: Science, v. 275(5301), p. 826-829, https://doi.org/10.1126/science.275.5301.826.

De Silva, S., Zandt, G., Trumbull, R., Viramonte, J.G., Salas, G. and Jiménez, N., 2006, Large ignimbrite eruptions and volcano-tectonic depressions in the Central Andes: a thermomechanical perspective: Geological Society, v. 269, p. 47-63, https://doi.org/10.1144/GSL.SP.2006.269.01.04.

De Silva, S.L., 1989, Altiplano-Puna volcanic complex of the central Andes: Geology, v. 17(12), p. 1102-1106.

Feeley, T.C., 1993, Crustal modification during subduction-zone magmatism: evidence from the southern Salar de Uyuni region (20-22 S), central Andes: Geology, v. 21, p. 1019-1022.

Fernandez, A.C., Hörmann, P.K., Kussmaul, S., Meave, J., Pichler, H., and Subieta, T., 1973, First petrologic data on young volcanic rocks of SW-Bolivia: Tschermaks mineralogische und petrographische Mitteilungen, v. 19, p. 149-172, https://doi.org/10.1007/BF01167425.

Francalanci, L., Tommasini, S., Conticelli, S., and Davies, G.R., 1999, Sr isotope evidence for short magma residence time for the 20th century activity at Stromboli volcano, Italy: Earth and Planetary Science Letters, v. 167, p. 61-69, https://doi.org/10.1016/S0012-821X(99)00013-8.

Francis, P.W. and De Silva, S.L., 1989, Application of the Landsat Thematic Mapper to the

identification of potentially active volcanoes in the Central Andes: Remote Sensing of Environment, v. 28, p. 245-255, https://doi.org/10.1016/0034-4257(89)90117-X.

Giletti, B.J. and Casserly, J.E.D., 1994, Strontium diffusion kinetics in plagioclase feldspars: Geochimica et Cosmochimica Acta, v. 58(18), p. 3785-3793, https://doi.org/10.1016/0016- 7037(94)90363-8.

Ginibre, C., Wörner, G., and Kronz, A., 2007, Crystal zoning as an archive for magma evolution: Elements, v. 3, p. 261-266, https://doi.org/10.2113/gselements.3.4.261.

Ginibre, C., Wörner, G., and Kronz, A., 2002, Minor-and trace-element zoning in plagioclase: implications for magma chamber processes at Parinacota volcano, northern Chile: Contributions to Mineralogy and Petrology, v. 143, p. 300-315, https://doi.org/10.1007/s00410-002- 0351-z.

Godoy, B., Wörner, G., Le Roux, P., de Silva, S., Parada, M.Á., Kojima, S., González-Maurel, O., Morata, D., Polanco, E. and Martínez, P., 2017, Sr-and Nd-isotope variations along the Pleistocene San Pedro–Linzor volcanic chain, N. Chile: Tracking the influence of the upper crustal Altiplano-Puna Magma Body: Journal of Volcanology and Geothermal Research, v. 341, p. 172-186, https://doi.org/10.1016/j.jvolgeores.2017.05.030.

Hickey, J., Gottsmann, J. and Del Potro, R., 2013. The large-scale surface uplift in the Altiplano-Puna region of Bolivia: A parametric study of source characteristics and crustal rheology using finite element analysis: Geochemistry, Geophysics, Geosystems, v. 14(3), p. 540-555, https://doi.org/10.1002/ggge.20057.

Hughes, G.E., Petrone, C.M., Downes, H., Varley, N.R., and Hammond, S.J., 2021, Mush remobilisation and mafic recharge: A study of the crystal cargo of the 2013–17 eruption at Volcán de Colima, Mexico: Journal of Volcanology and Geothermal Research, v. 416, p. 107296, https://doi.org/10.1016/j.jvolgeores.2021.107296.

Jordán, T.E., Isacks, B.L., Allmendinger, R.W., Brewer, J.A., Ramos, V.A., and Ando, C.J., 1983, Andean tectonics related to geometry of subducted Nazca plate: Geological Society of America Bulletin, v. 94, p. 341-361.

Kern, J.M., de Silva, S.L., Schmitt, A.K., Kaiser, J.F., Iriarte, A.R. and Economos, R., 2016, Geochronological imaging of an episodically constructed subvolcanic batholith: U-Pb in zircon chronochemistry of the Altiplano-Puna Volcanic Complex of the Central Andes: Geosphere, v. 12(4), p. 1054-1077, https://doi.org/10.1130/GES01258.1.

Kussmaul, S., Hörmann, P.K., Ploskonka, E., and Subieta, T., 1977, Volcanism and structure of southwestern Bolivia: Journal of Volcanology and Geothermal Research, v. 2, p.73-111, https://doi.org/10.1016/0377-0273(77)90016-6.

Lieu, W.K. and Stern, R.J., 2019, The robustness of Sr/Y and La/Yb as proxies for crust thickness in modern arcs: Geosphere, v. 15, p. 621-641, https://doi.org/10.1130/GES01667.1.

Lubbers, J., Kent, A.J. and de Silva, S., 2022, Thermal budgets of magma storage constrained by diffusion chronometry: the Cerro Galán ignimbrite: Journal of Petrology, v. 63(7), https://doi.org/10.1093/petrology/egac048.

Mamani, M., Wörner, G., and Sempere, T., 2010, Geochemical variations in igneous rocks of the Central Andean orocline (13 S to 18 S): Tracing crustal thickening and magma generation through time and space: GSA Bulletin, v. 122, p. 162-182, https://doi.org/10.1130/B26538.1.

McDonough, W.F. and Sun, S.S., 1995, The composition of the Earth: Chemical geology, v. 120, p. 223-253, https://doi.org/10.1016/0009-2541(94)00140-4.

Michelfelder, G.S., Feeley, T.C., and Wilder, A.D., 2014, The volcanic evolution of Cerro Uturuncu: A high-K, composite volcano in the back-arc of the Central Andes of SW Bolivia: International Journal of Geosciences, v. 5, p. 1263, https://doi.org/10.4236/ijg.2014.511105.

Michelfelder, G.S., Feeley, T.C., Wilder, A.D., and Klemetti, E.W., 2013, Modification of the continental crust by subduction zone magmatism and vice-versa: Across-strike geochemical variations of silicic lavas from individual eruptive centers in the Andean Central volcanic zone: Geosciences, v. 3, p. 633-667, https://doi.org/10.3390/geosciences3040633.

Muir, D. D., Barfod, D.N., Blundy, J.D., Rust, A.C., Sparks, R.S.J., and Clarke, K.M., 2015, The Temporal Record of Magmatism at Cerro Uturuncu, Bolivian Altiplano: Geological Society, London, Special Publications, v. 422, p. 57–83, https://doi.org/10.1144/sp422.1.

Muir, D.D., Blundy, J.D., Hutchinson, M.C., and Rust, A.C., 2014, Petrological imaging of an active pluton beneath Cerro Uturuncu, Bolivia: Contributions to Mineralogy and Petrology, v. 167, p. 980, https://doi.org/10.1007/s00410-014-0980-z.

Muir, D.D., Blundy, J.D., Rust, A.C., and Hickey, J., 2014, Experimental constraints on dacite pre-eruptive magma storage conditions beneath Uturuncu volcano: Journal of Petrology, v. 55, p. 749-767, https://doi.org/10.1093/petrology/egu005.

Paton, C., Hellstrom, J., Paul, B., Woodhead, J. and Hergt, J., 2011, Iolite: Freeware for the visualisation and processing of mass spectrometric data: Journal of Analytical Atomic Spectrometry, v. 26, p. 2508-2518, https://doi.org/10.1039/C1JA10172B.

Pritchard, M.E., De Silva, S.L., Michelfelder, G., Zandt, G., McNutt, S.R., Gottsmann, J., West, M.E., Blundy, J., Christensen, D.H., Finnegan, N.J., and Minaya, E., 2018, Synthesis: PLUTONS: Investigating the relationship between pluton growth and volcanism in the Central Andes: Geosphere, v. 14, p. 954-982, https://doi.org/10.1130/GES01578.1.

Renjith, M.L., 2014, Micro-textures in plagioclase from 1994–1995 eruption, Barren Island Volcano: evidence of dynamic magma plumbing system in the Andaman subduction zone: Geoscience frontiers, v. 5(1), p.113-126, https://doi.org/10.1016/j.gsf.2013.03.006.

Scott, E.M., Allen, M.B., Macpherson, C.G., McCaffrey, K.J., Davidson, J.P., Saville, C. and Ducea, M.N., 2018, Andean surface uplift constrained by radiogenic isotopes of arc lavas: Nature communications, v. 9, p.1-8, https://doi.org/10.1038/s41467-018-03173-4.

Sparks, R.S.J., Folkes, C.B., Humphreys, M.C., Barfod, D.N., Clavero, J., Sunagua, M.C., McNutt, S.R., and Pritchard, M.E., 2008, Uturuncu volcano, Bolivia: Volcanic unrest due to mid-crustal magma intrusion: American Journal of Science, v. 308, p. 727-769, https://doi.org/10.2475/06.2008.01.

Tassara, A., Götze, H.J., Schmidt, S., and Hackney, R., 2006, Three-dimensional density model of the Nazca plate and the Andean continental margin: Journal of Geophysical Research: Solid Earth, v. 111, https://doi.org/10.1029/2005JB003976.

Tepley III, F.J., Lundstrom, C.C., McDonough, W.F. and Thompson, A., 2010, Trace element partitioning between high-An plagioclase and basaltic to basaltic andesite melt at 1 atmosphere pressure: Lithos, v. 118(1-2), p. 82-94, https://doi.org/10.1016/j.lithos.2010.04.001.

Tepley III, F.J., Davidson, J.P., Tilling, R.I. and Arth, J.G., 2000, Magma mixing, recharge and eruption histories recorded in plagioclase phenocrysts from El Chichon Volcano, Mexico: Journal of Petrology, v. 41(9), p. 1397-1411, https://doi.org/10.1093/petrology/41.9.1397.

Tepley III, F.J., Davidson, J.P. and Clynne, M.A., 1999, Magmatic interactions as recorded in plagioclase phenocrysts of Chaos Crags, Lassen Volcanic Center, California: Journal of Petrology, v. 40(5), p. 787-806, https://doi.org/10.1093/petroj/40.5.787.

Viccaro, M., Giuffrida, M., Nicotra, E., and Ozerov, A.Y., 2012, Magma storage, ascent and recharge history prior to the 1991 eruption at Avachinsky Volcano, Kamchatka, Russia: Inferences on the plumbing system geometry: Lithos, v. 140, p. 11-24, https://doi.org/10.1016/j.lithos.2012.01.019.

Ward, K.M., Zandt, G., Beck, S.L., Christensen, D.H. and McFarlin, H., 2014, Seismic imaging of the magmatic underpinnings beneath the Altiplano-Puna volcanic complex from the joint inversion of surface wave dispersion and receiver functions: Earth and Planetary Science Letters, v. 404, p. 43-53, https://doi.org/10.1016/j.epsl.2014.07.022.

Ward, K.M., Porter, R.C., Zandt, G., Beck, S.L., Wagner, L.S., Minaya, E. and Tavera, H., 2013, Ambient noise tomography across the Central Andes: Geophysical Journal International, v. 194, p. 1559-1573, https://doi.org/10.1093/gji/ggt166.

Woodhead, J.D., Hellstrom, J., Hergt, J.M., Greig, A. and Maas, R., 2007, Isotopic and elemental imaging of geological materials by laser ablation inductively coupled plasma-mass spectrometry: Geostandards and Geoanalytical Research, v. 31, p. 331-343, https://doi.org/10.1111/j.1751-908X.2007.00104.x.

Yuan, X., Sobolev, S.V., and Kind, R., 2002, Moho topography in the central Andes and its

geodynamic implications: Earth and Planetary Science Letters, v. 199, p. 389-402, https://doi.org/10.1016/S0012-821X(02)00589-7.

Zandt, G., Leidig, M., Chmielowski, J., and Baumont, D., 2003, Seismic detection and characterization of the Altiplano-Puna magma body, Central Andes: Pure and Applied Geophysics, v. 160, p. 789–807, https://doi.org/10.1007/PL00012557.

Zellmer, G.F., Blake, S., Vance, D., Hawkesworth, C., and Turner, S., 1999, Plagioclase residence times at two island arc volcanoes (Kameni Islands, Santorini, and Soufriere, St. Vincent) determined by Sr diffusion systematics: Contributions to Mineralogy and Petrology, v. 136, p.345-357, https://doi.org/10.1007/s004100050543.
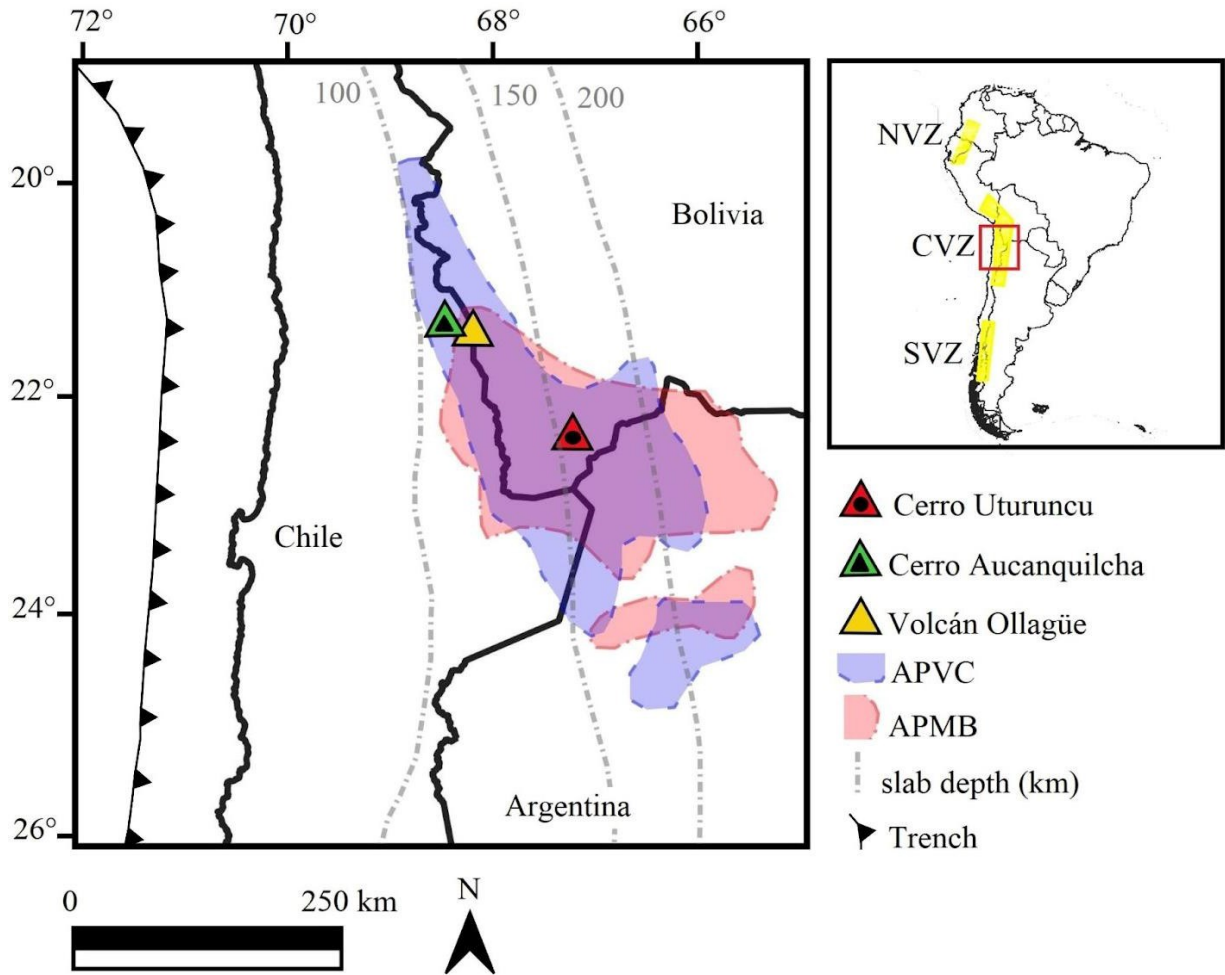
Figure 1. Regional map of Cerro Uturuncu with respect to two front arc volcanoes, Cerro Aucanquilcha and Volcán Ollagüe, within the Andean Central Volcanic Zone (CVZ). The approximate boundary of the Altiplano Puna Volcanic Complex (APVC) and Altiplano Puna Magma Body (APMB) are outlined. Modified from Muir et al. (2014).
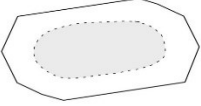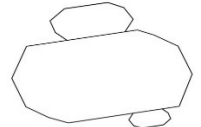
Texture	Description & Interpretation
Spongy Core	Large inclusions of glass, microlites, or Fe-Ti oxides in the center of the plagioclase. The texture is caused by decompression melting.
Sieved Rim	Small inclusions of glass, microlites, or Fe-Ti oxides at the rim of the plagioclase. The texture is caused by a reaction between the plagioclase and hotter Ca-rich magma.
Resorption Surface	A boundary between two growth zones wherein original growth from the core has been dissolved. The texture is caused by extensive dissolution and interaction with a parental magma.
Fine Zoning	The oscillatory change between differing X_{An} compositions. The texture is caused by consistent oscillation of temperature through small-scale convection within the magma chamber.
Synneusis	The attachment of plagioclase grains on their respective planar fascia. The texture is caused by unstable magma conditions attributed to convection within the magma chamber.

Figure 2. Illustrations, descriptions, and interpretations of commonly observed plagioclase textures within Cerro Uturuncu samples.
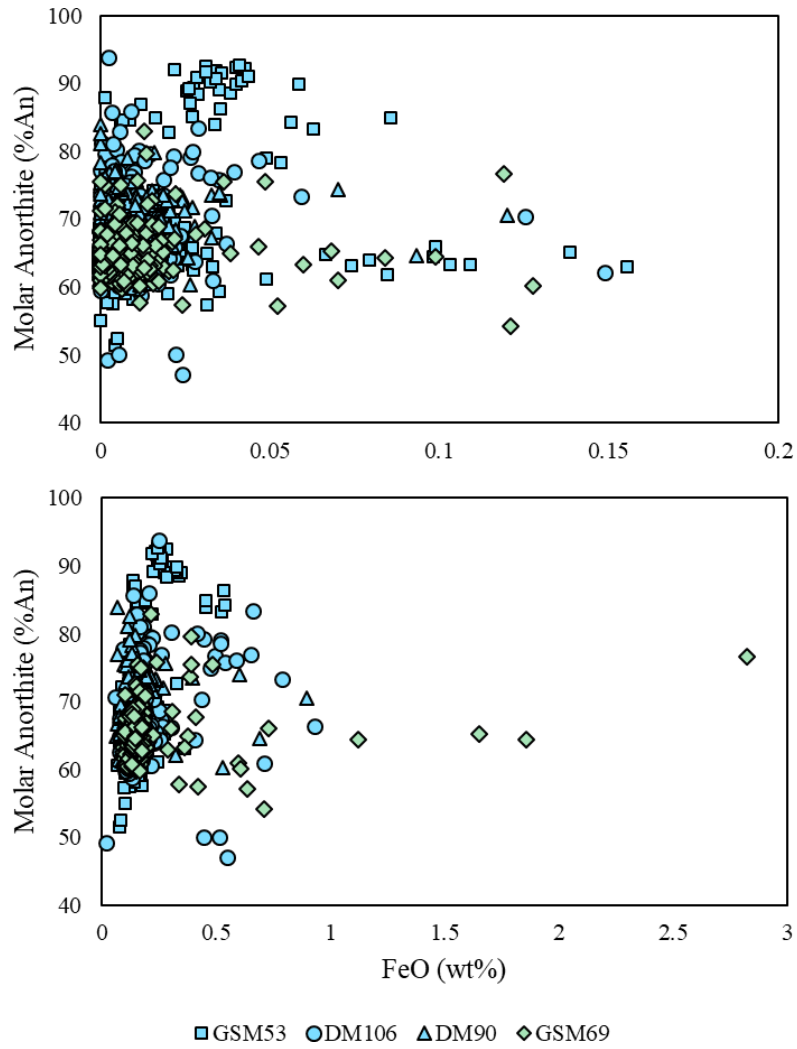
Figure 3. MgO and FeO (wt%) versus molar Anorthite percentage for Puntas Negras (UTUGSM53, UTDM106, and UTDM90; shown in blue squares, circles, and triangles) and Uturuncu (UTUGSM69; shown in green diamonds) stage plagioclase.
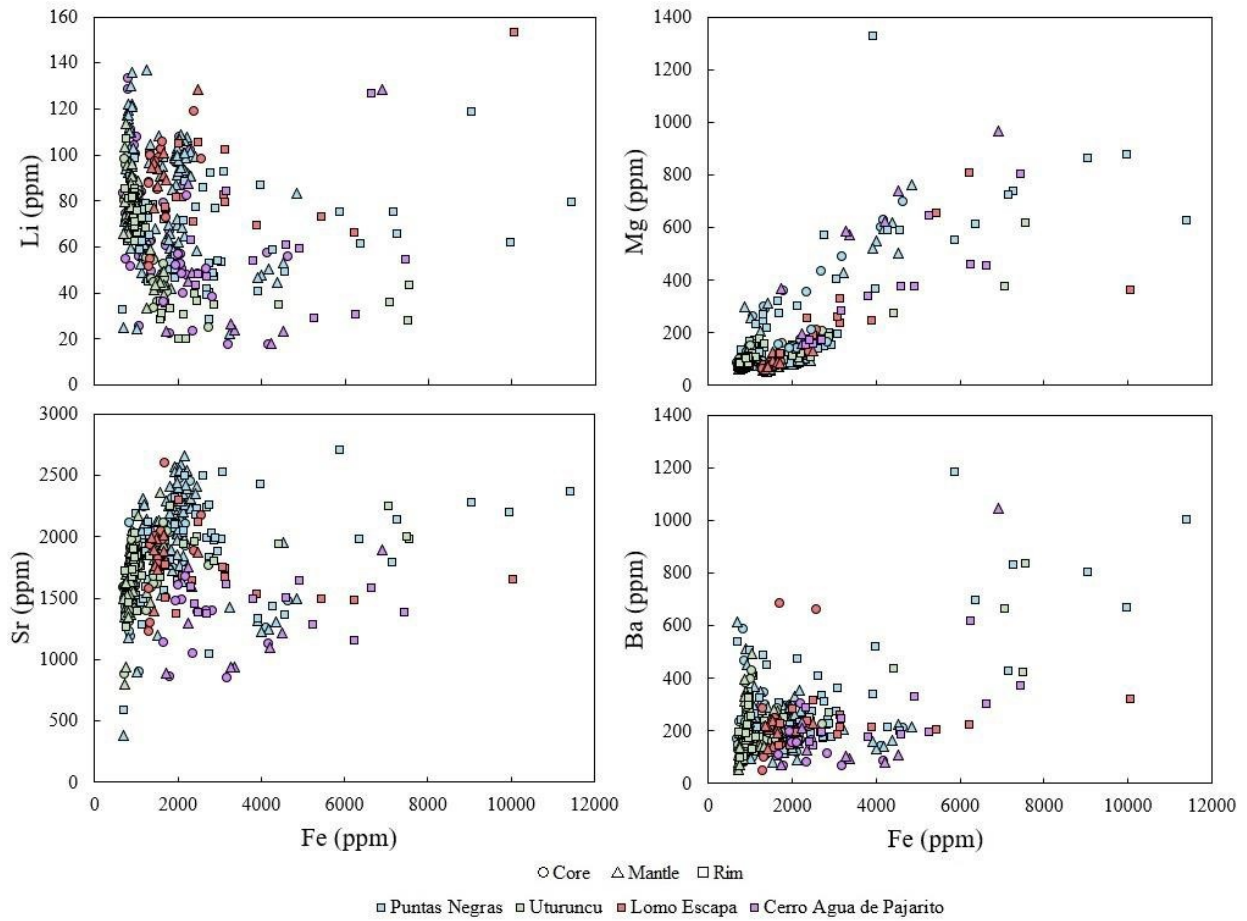
Figure 4. Trace element comparison (Li, Mg, Sr, and Ba versus Fe) of Cerro Agua de Pajarito, Lomo Escapa, Uturuncu, and Puntas Negras stages.
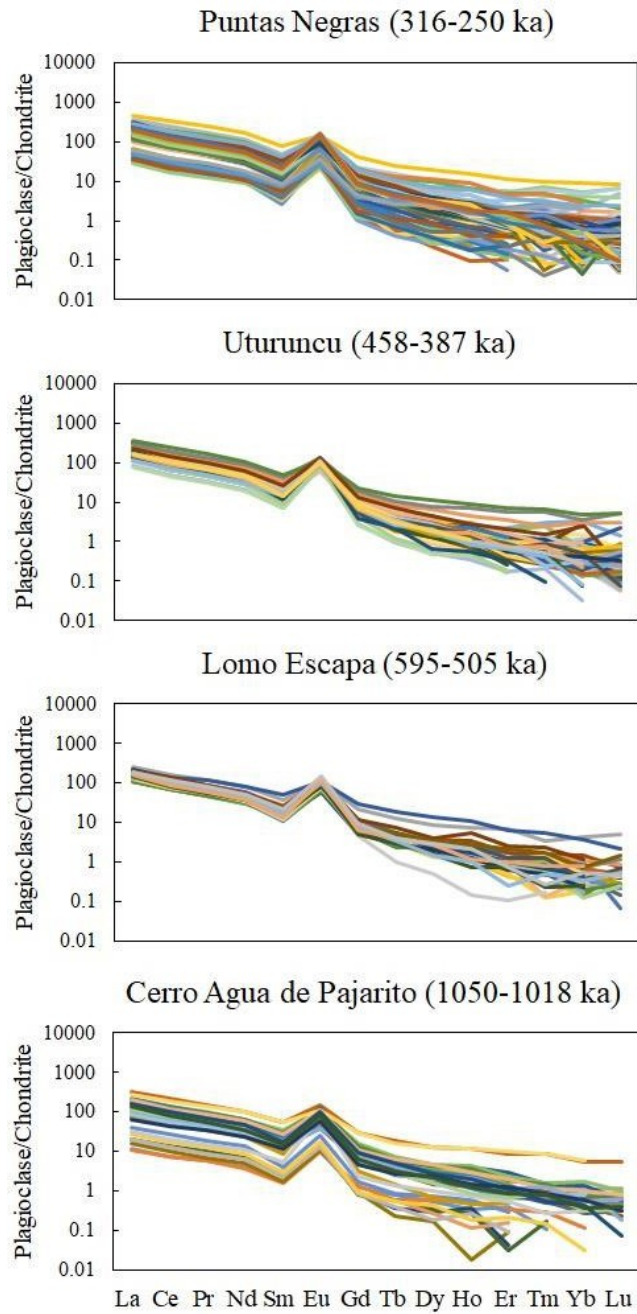
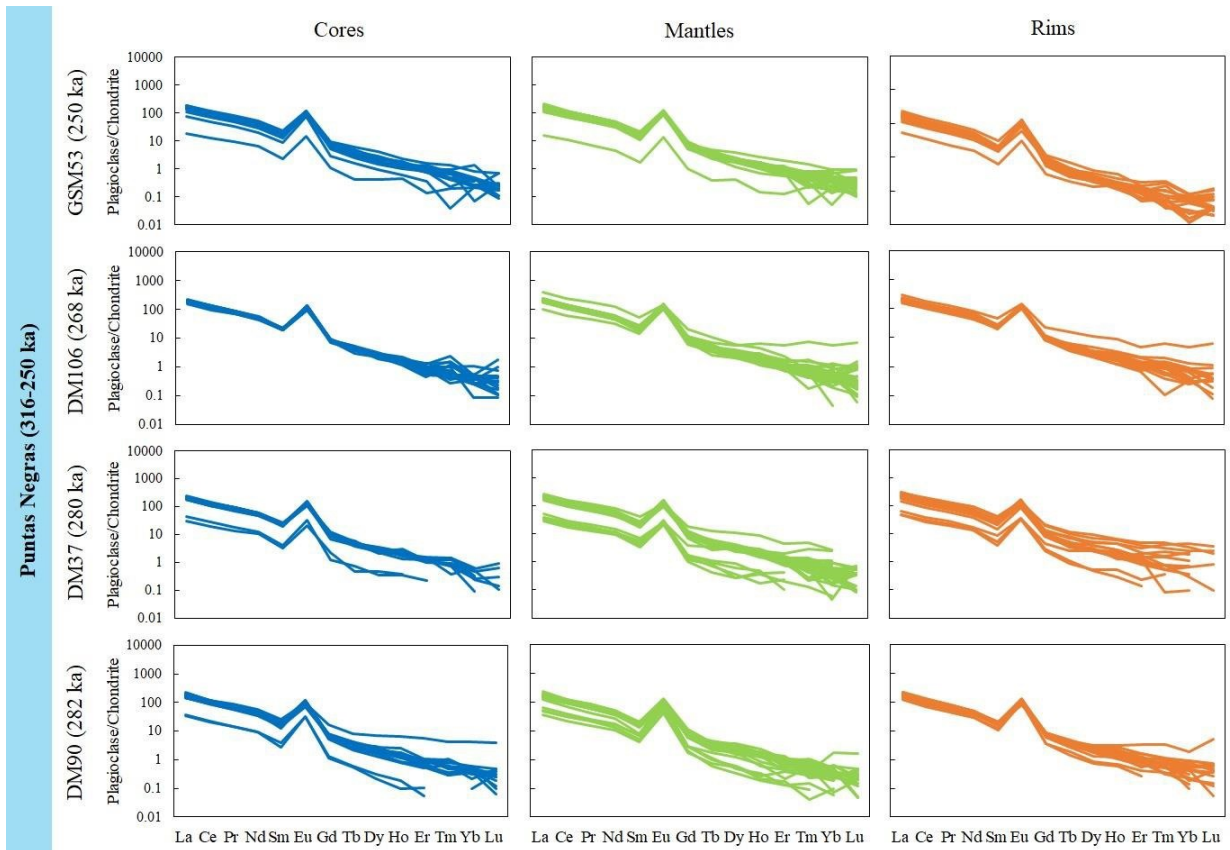**Figure 5.** Rare earth element (REE) diagrams for Cerro Agua de Pajarito, Lomo Escapa, Uturuncu, and Puntas Negras stages.

Figure 6. REE diagram for Puntas Negras samples (UTUGSM53, UTDM106, UTDM37, and UTDM90) separated into cores, mantles, and rims.
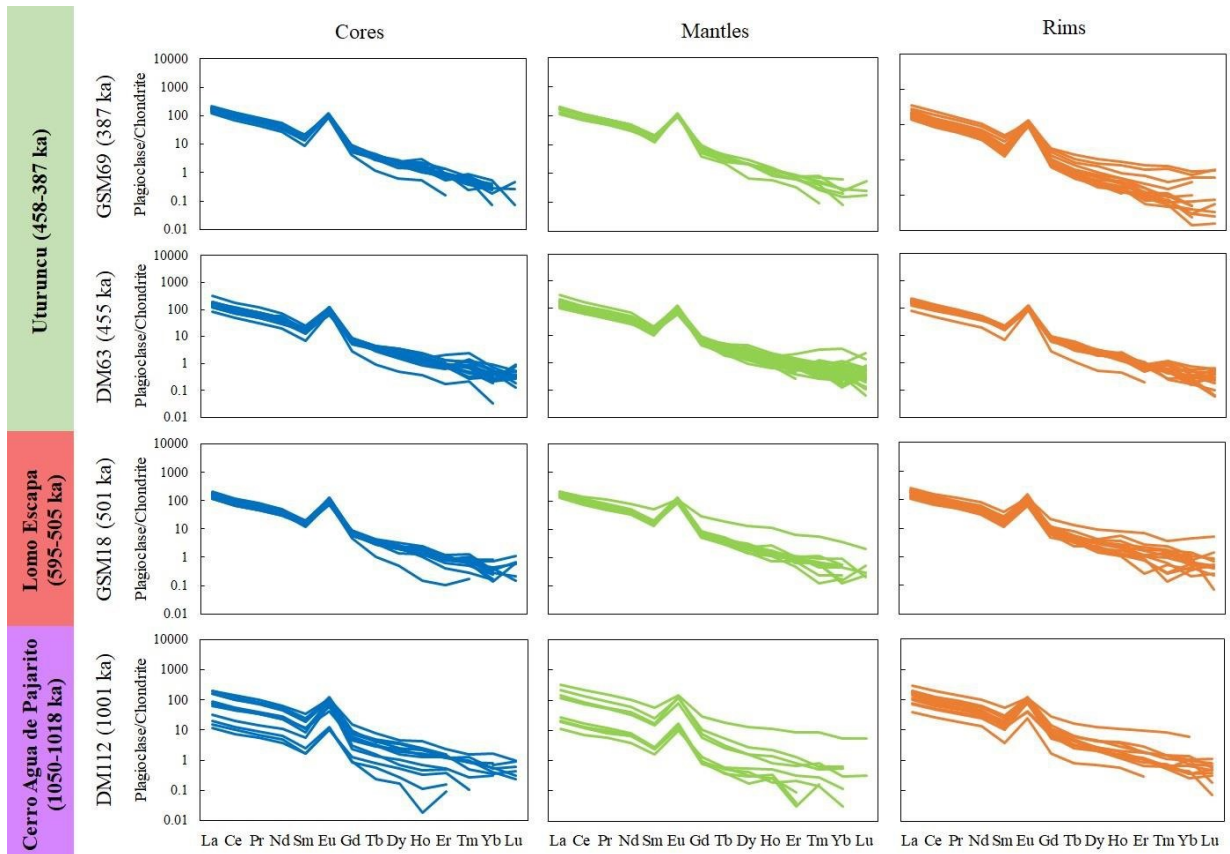
Figure 7. REE diagram for Cerro Agua de Pajarito sample (UTDM112), Lomo Escapa sample (UTUGSM18), and Uturuncu samples (UTUGSM69 and UTDM63).
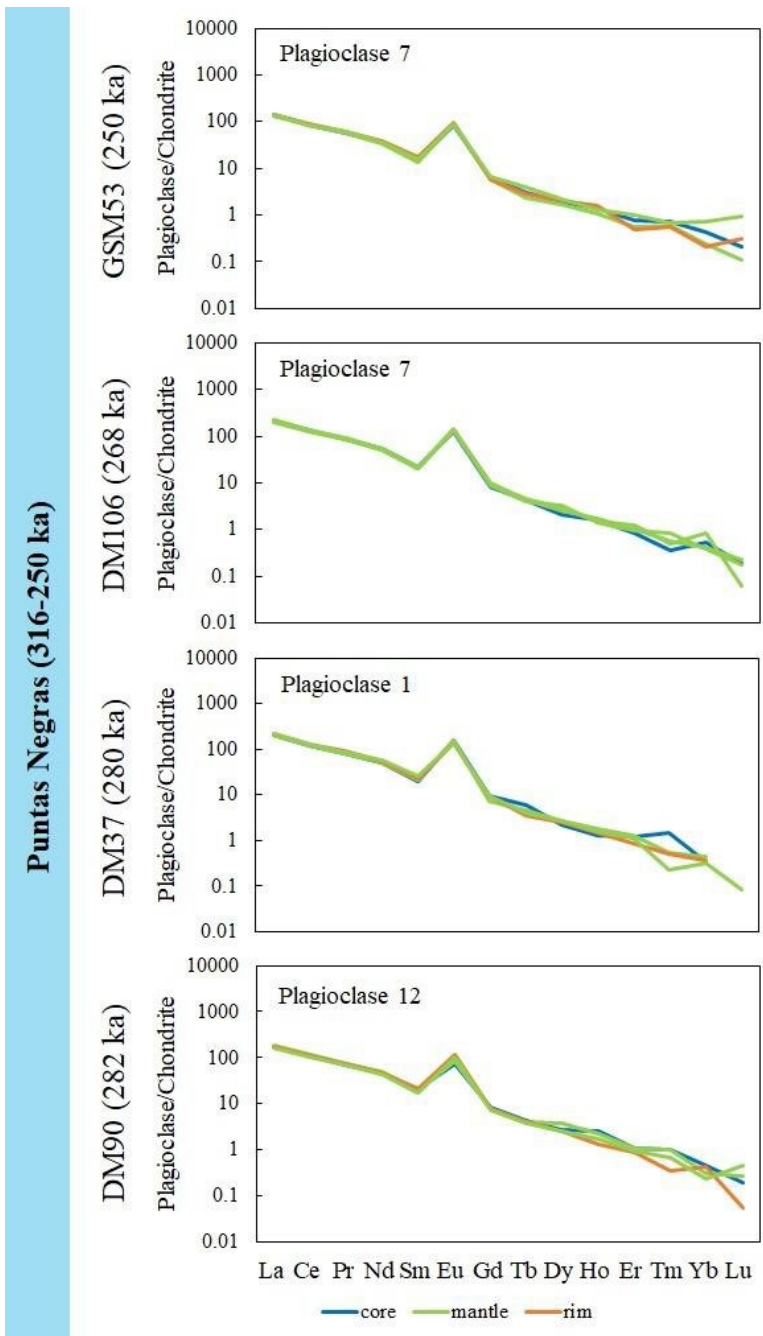
Figure 8. Puntas Negras REE diagrams for an example plagioclase phenocryst for each selected sample (UTDM90, UTDM106, UTUGSM53, UTDM37).
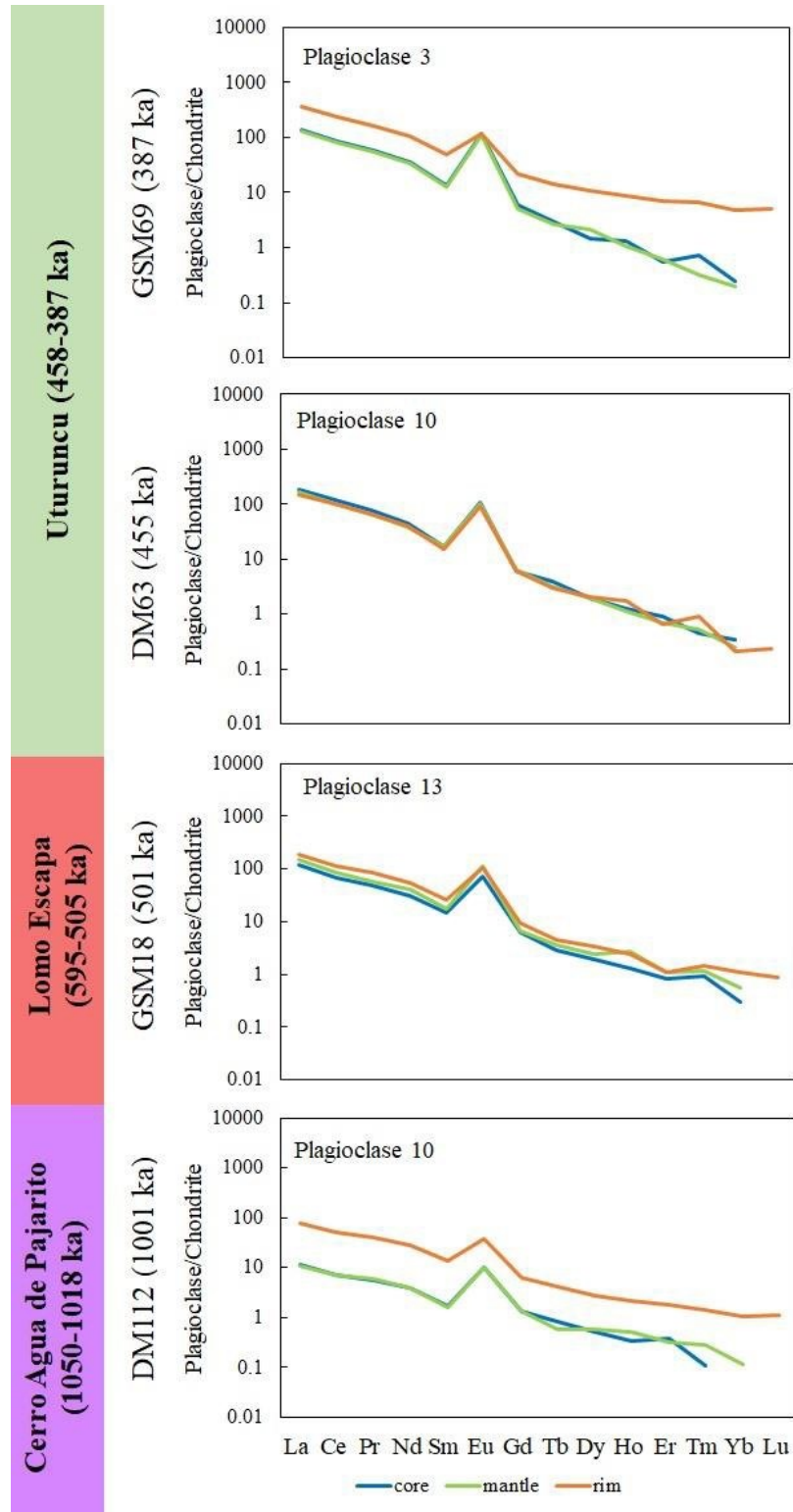
Figure 9. Cerro Agua de Pajarito, Lomo Escapa, and Uturuncu REE diagrams for an example plagioclase phenocryst for each selected sample (UTDM112; UTUGSM18; UTDM63, UTUGSM69).
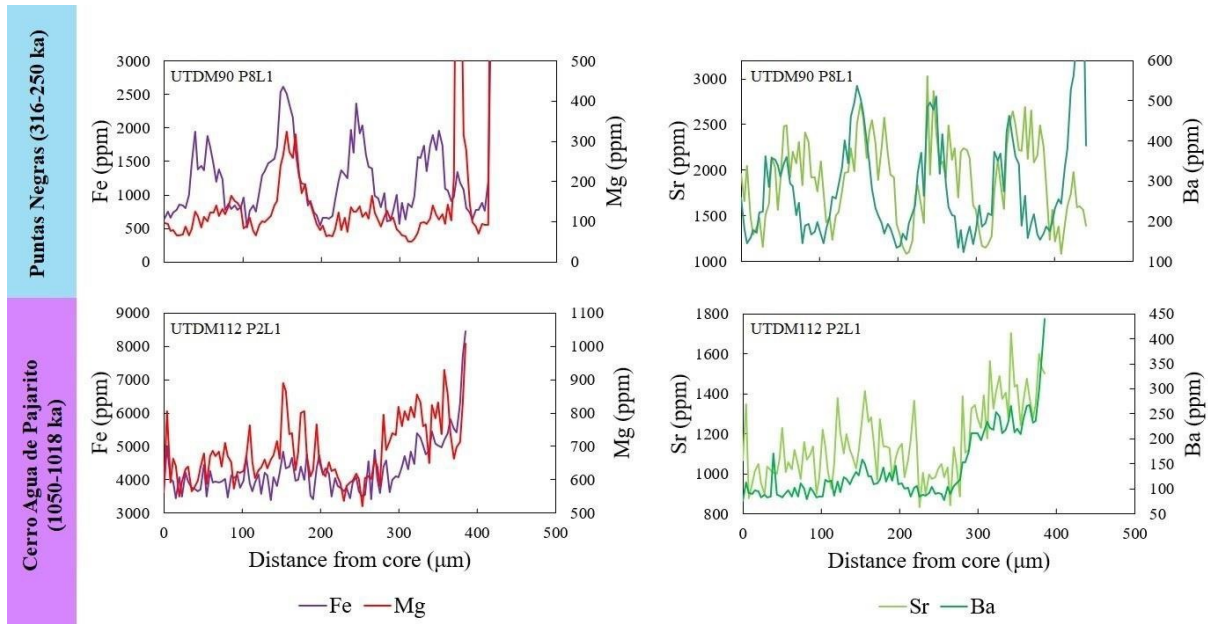
Figure 10. Iron and Mg line transect and Sr and Ba line transect examples for Puntas Negras and Cerro Agua de Pajarito stage samples. Fe and Sr concentrational trends are followed by Mg and Ba, respectively.
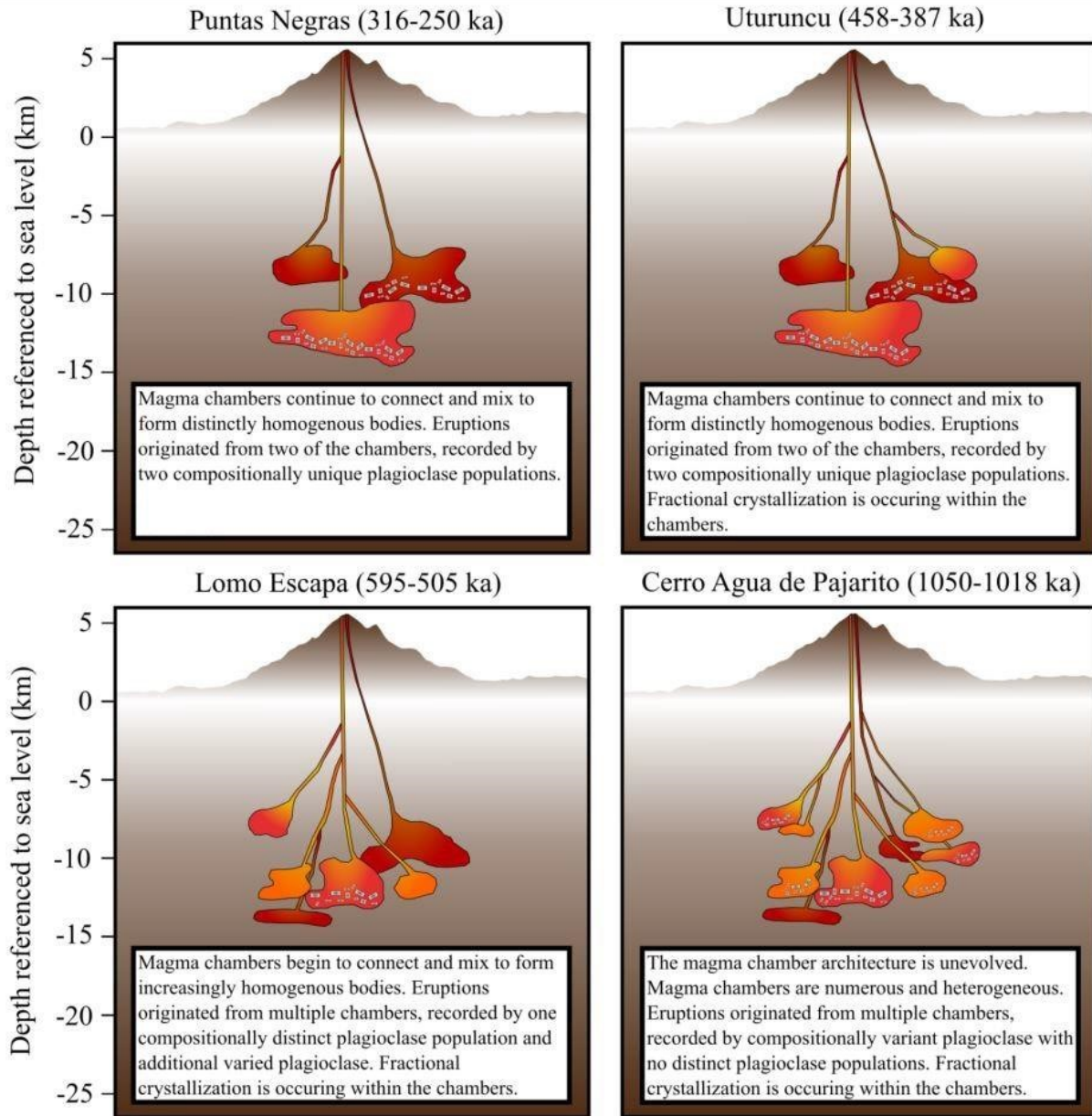
Figure 11. Proposed underlying magma plumbing architecture for Cerro Uturuncu. From 1050 ka to 250 ka, the magma chambers evolve from many heterogeneous bodies to few individually homogenous bodies. Fractional crystallization occurs within these bodies throughout its history.
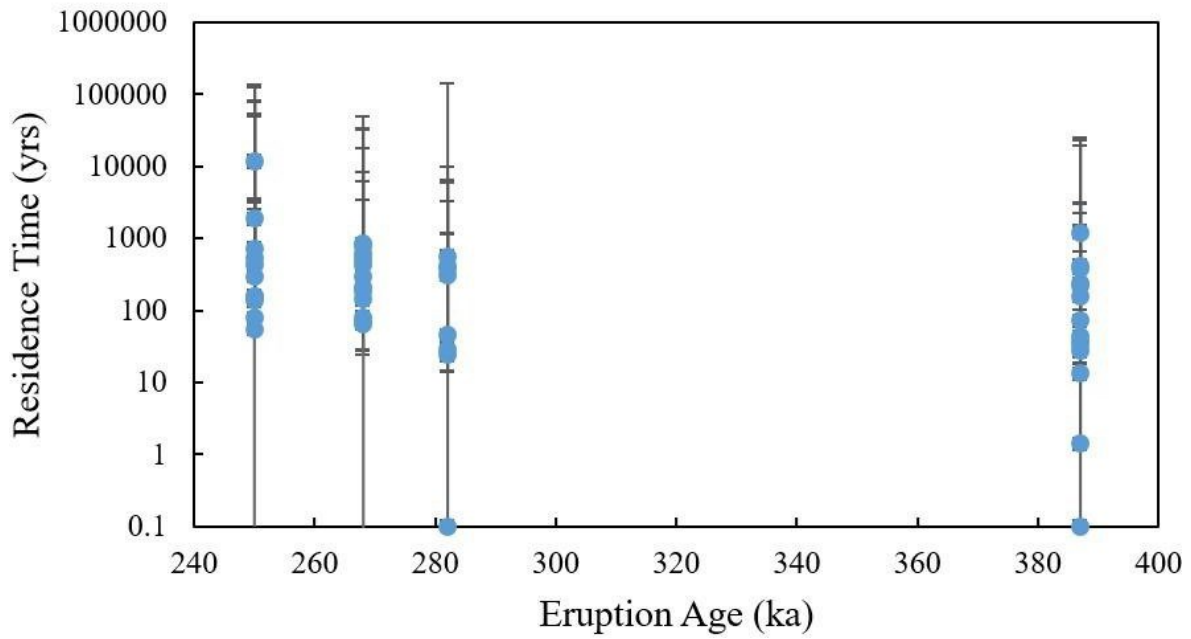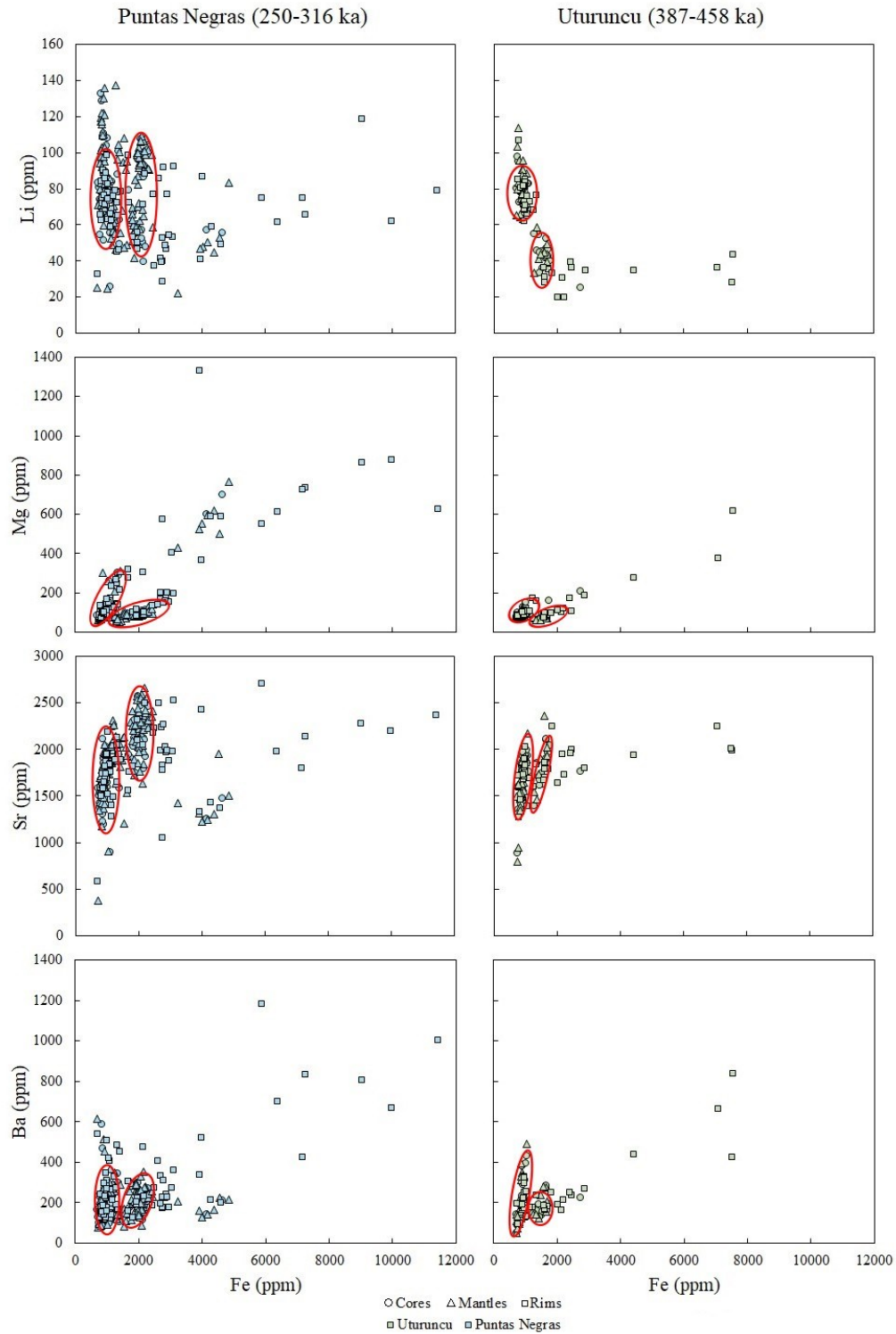
Figure 12. Sr diffusion modeling residence times (modeled at 770C) compared to eruption ages for samples UTUGSM53, UTDM106, UTDM90, and UTUGSM69. Error bars indicate 2σ values.
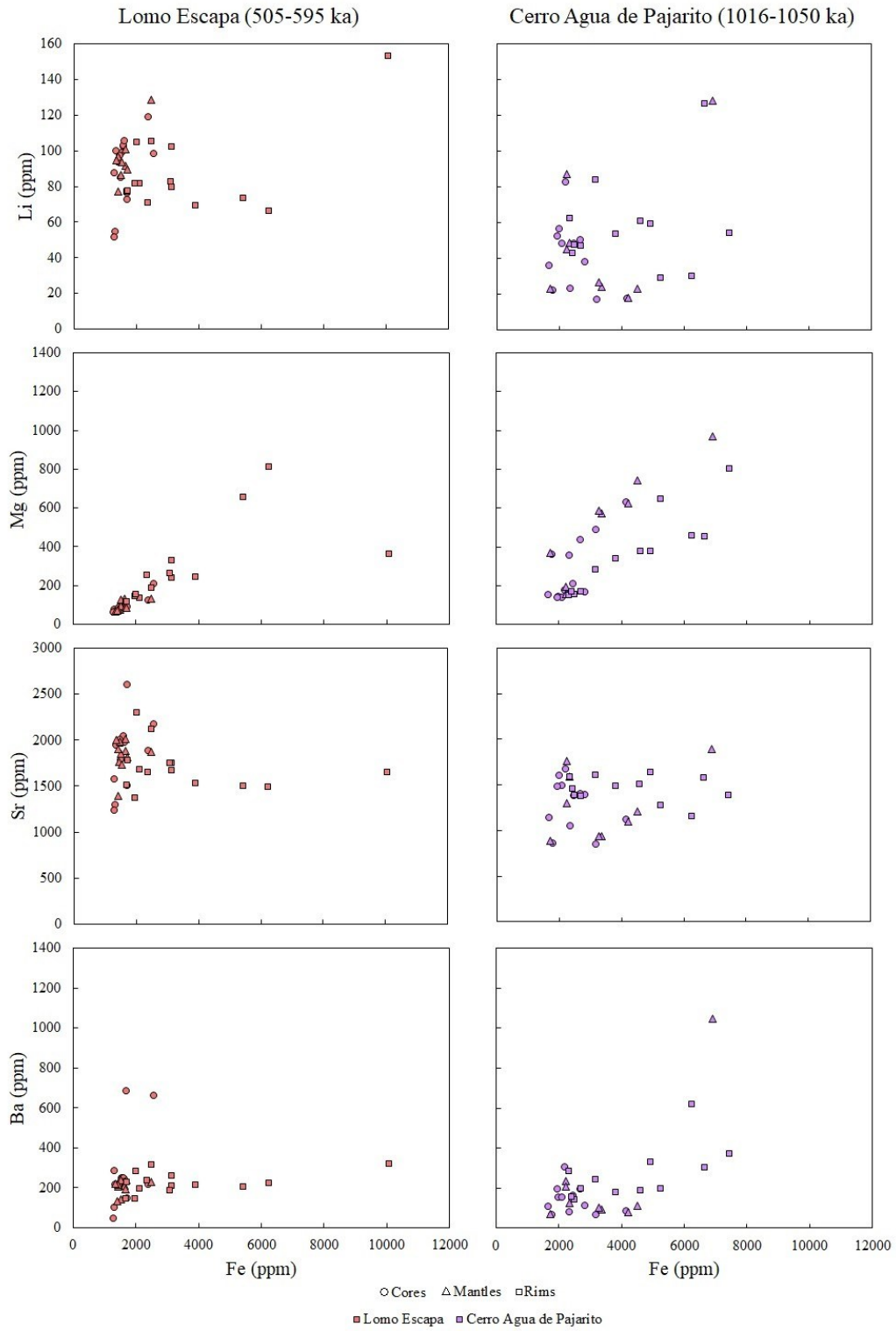
Appendix A.

Trace Element Comparison Across Stages. Figure 1 separated into trace element comparison (Li, Mg, Sr, and Ba versus Fe) by stage (Uturuncu and Puntas Negras). Red ovals indicate clustering.

Appendix B.

Trace Element Comparison Across Stages. Figure 1 separated into trace element comparison (Li, Mg, Sr, and Ba versus Fe) by stage (Cerro Agua de Pajarito and Lomo Escapa).